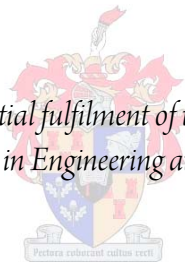


The development of equipment for the fabrication of thin film superconductor and nano structures

by

Ulrich Büttner

*Thesis presented in partial fulfilment of the requirements for the degree
Master of Science in Engineering at Stellenbosch University*



Supervisor: Prof WJ Perold
Department of Electrical & Electronic Engineering

March 2011

Declaration

By submitting this thesis electronically, I declare that the entirety of the work contained therein is my own original work, that I am the sole author thereof (save to the extent explicitly otherwise stated), that reproduction and publication thereof by Stellenbosch University will not infringe any third party rights and that I have not previously in its entirety or in part submitted it for obtaining any qualification.

Date: March 2011

Abstract

The development of equipment for the fabrication of thin film superconductor and nano structures

U. Büttner

*Department of Electrical and Electronic Engineering
Stellenbosch University
Private Bag X1, 7602 Matieland, South Africa*

Thesis: MScEng (E and E)

December 2010

The nano-age is more about the mesoscopic phenomena, than those occurring at molecular and atomic level, which have been studied by chemists and physicists for more than a hundred years. Nanotechnology is currently one of the most active fields being explored in many different disciplines by many scientists across the world. In this research field, it is imperative to continually create more effective and superior methods to build smaller and smaller electronic devices, circuits and sensors. Technology is being improved continually and, specifically at our university, there was a need to improve our device manufacturing facility. The aim of this work was to create a new sputtering system, build a dry etching system and to make modifications to upgrade existing equipment. This work has been done to produce nano structures or devices and, most importantly, to save costs.

New systems and equipment have been built to keep up with the progress in this field. In order to understand the significance of the different types of equipment used in the fabrication of thin film superconductor layers, an overview will be given of the complete process of manufacturing a patterned Josephson junction. The apparatus used will be described and critically analyzed, whereby the shortfalls in design will be highlighted and improvements shown. Some of the equipment, such as the plasma laser deposition system, the lithography system and the test facility existed before and has been modified. Newly designed systems were built to further improve the quality of our thin film superconductors; these include the inverted cylindrical magnetron (ICM) sputtering system, the argon ion mill and the incandescent substrate heater.

Finally, the results of the improved thin films and structures will be shown. To summarize: The entire process was analyzed and upgraded, resulting in an improved device manufacturing facility.

Opsomming

Die nano-era het aangebreek en nanotegnologie is tans een van die mees aktiewe en diverse navorsingsvelde wat wetenskaplikes wêreldwyd ontgin - hoofsaaklik as gevolg van nuwe verskynsels op molekulêre en atomiese vlak. In die nanotegnologie-navorsingsveld is die vereiste dat daar voortdurend meer effektiewe metodes gevind moet word om die al hoe meer miniatuurwordende elektroniese meganismes met verbeterde energieverbruik, spoed en ruimtebesparende vermoëns tot stand te bring.

Dit is duidelik dat in hierdie toonaangewende navorsingsveld, waar tegnologiese ontwikkeling voorturend en snelgroeiend is, dit dikwels vinniger is om reeds bestaande toerusting aan te pas en te moderniseer ten einde in pas te bly met nuutontwikkelde en ontwikkelende tegnologieë. Die doel van die werk verrig, wat hier beskryf word, was om 'n nuwe deponeerstelsel, sowel as 'n droogets stelsel te bou. Bestaande apparaat is opgradeer deur verandering aan te bring. Die uiteintelike doel is die vervaardiging van beter nano-strukture, en terselfde tyd om kostes te bespaar.

Nuwe stelsels en toerusting is gebou om tred te hou met tegnologiese vooruitgang. Om die belangrikheid van die verskillende tipes toerusting wat in die vervaardiging van dunlaag- supergeleierlae gebruik word te verstaan, sal 'n oorsig van die volledige vervaardigingsproses van 'n Josephson-patroon gegee word. Die apparaat wat gebruik is, sal beskryf en krities ontleed word en die tekorte in ontwerp sal uitgelig word, terwyl verbeterings aangetoon sal word. Sommige van die toerusting het voorheen bestaan en is aangepas, byvoorbeeld die plasmalaser-neerleggingstelsel, die litografiestelsel en die toetsfasiliteit. Nuwe ontwerpstelsels is gebou om die gehalte van ons dunlaagsupergeleiers verder te verbeter. Dit sluit die silindriese plasma deponeer stelsel, die Argon-ioon bron en die substraatverwarmer in.

In hierdie tesis word daar eerstens 'n oorsig gegee van die totstandkomingsproses van 'n supergeleier kwantum-interferensiemeganisme, beginnende met dunlaagneerslag van YBCO (Yttrium, Barium en Koperoksied). Die oorsig word gevolg deur 'n stap-vir-stap beskrywing van elke daaropvolgende proses wat lei tot die voltooiing van die meganisme. Daarna word die toetsprosedure van die dunlaag en instrumente verduidelik. Bykomende veranderinge wat aan bestaande instrumente aangebring is (ten einde die dunfilmlae te verbeter en die toetsfasiliteit op te gradeer) word ook bespreek.

Daar sal ook verwys word na artikels wat in verskeie joernale verskyn het oor die vernuwende aanpassings en sisteme wat in hierdie tesis verduidelik word. Ten slotte sal die resultate van die verbeterde dunlae en strukture getoon word. Kortom: die hele

proses is ontleed en opgegradeer om 'n verbeterde apparaatvervaardigingsfasiliteit tot gevolg te hê.

Acknowledgements

I would like to express my sincere gratitude to the following people without whom this thesis would not have been possible. To my supervisor Prof. W.J. Perold: Thank you for your positive support, encouragement and guidance in enabling me to complete this work.

To Prof. V.V. Srinivasu, who has been a great help in the analysis of the laser junction tunneling and constriction effects, and ultimately bringing this work to publication.

To the Physics Department (LRI), especially Prof. H. von Bergmann and Prof. E. Rohwer and Uli Deutschlaender for their support and for maintaining the excimer laser.

I would like to thank Pieter de Kock for his assistance, especially in the work done on the ion mill RF matching circuit design, e-beam software and the design and building of a temperature controller as well as his support in many ways.

I would also like to thank my colleagues Wessel Croukamp, Lincoln Saunders and Ashley Cupido for their loyalty, assistance and encouragement.

To Jackie Blom and his team, thank you for assisting me with the technical diagrams and construction of the ion argon mill and various modifications on the PLD system.

To my colleague and friend, the late Willie van Rooyen, who was instrumental in designing the test equipment for measuring the susceptibility of the YBCO thin films: he was a great inspiration to me and will be dearly missed.

To the SAND group for assisting me in using some software packages. A special thanks to Graham, Akram, Niel, Migael, Arnoux, Derrick, Nicky, Carlo and Stanley for all their support.

To my dearest wife, Cathy, who has been supportive and inspirational throughout this time and encouraged me to pursue this work. Thank you to all my family.

Contents

Declaration	i
Abstract	ii
Opsomming	iv
Acknowledgements	vi
Contents	vii
List of Figures	x
List of Tables	xiv
Nomenclature	xvi
1 Foundations of Superconductor and Thin Film Fabrication	1
1.1 History	1
1.2 Thin Films	2
1.2.1 Physical Sputter Deposition	3
1.2.2 Sputter Energy Dependence	3
1.2.3 Pulsed Laser Deposition	4
1.2.4 Laser Assisted Molecular Beam Deposition	5
1.2.5 Chemical Vapour Deposition	5
1.3 Conclusion	6
2 YBCO Device Fabrication Process	8
2.1 Introduction	8
2.1.1 Substrate Choice and Preparation	8
2.1.2 Thin Film Deposition	9
2.1.3 Analysis of Thin Films	12
2.1.4 Spin Coating	12
2.1.5 Soft-Baking	13
2.1.6 Optical Ultra Violet Photolithography	13
2.1.7 Photoresist Developing	14
2.1.8 Post-Baking	15
2.1.9 Chemical Wet Etching	15
2.1.10 Argon Ion Milling	15
2.1.11 Contact Pads	17

2.1.12	Testing the Superconductor Device	17
2.2	Conclusion	19
3	Pulsed Laser Deposition	20
3.1	Introduction	20
3.1.1	Experiment Parameters	21
3.1.2	Chamber Considerations	22
3.1.3	Target	22
3.1.4	Laser Density	23
3.1.5	Base Pressure	23
3.1.6	Gas Pressure	24
3.1.7	Target To Substrate Distance	24
3.1.8	Pulse Repetition Rate	24
3.1.9	Substrate Temperature	25
3.2	Problem Identification and Solutions	25
3.2.1	Multiple Substrate Holder	26
3.2.2	Design Considerations	26
3.2.3	PLD with Shadow Mask	27
3.2.4	Laser Assisted Molecular Beam Deposition	28
3.2.5	Pulsed Reactive Crossed Beam Laser Ablation	29
3.3	Conclusion	31
4	Inverted Cylindrical Magnetron Sputtering	33
4.1	Motivation	33
4.1.1	Basic Vacuum Considerations	34
4.1.2	Target Selection	34
4.1.3	Magnet Design	34
4.1.4	Water Cooling	35
4.1.5	Material Selection	36
4.1.6	Dual Sputtering Magnet Design	37
4.1.7	Substrate Heater	37
4.2	Results of analysis of YBCO thin film and oxygen/argon reactive gas mix	39
4.3	Conclusions	40
5	Argon Ion Mill	41
5.1	Introduction To Argon Ion Milling	41
5.1.1	Basic Design	41
5.1.2	Modifications On The Plasma Extraction	42
5.1.3	Vacuum Considerations	44
5.1.4	Magnetic Plasma Containment	44
5.1.5	High Voltage Requirements	45
5.1.6	Water Cooling	46
5.1.7	RF Antenna Matching	46
5.1.8	Substrate Holder	46
5.1.9	RF Shielding	48
5.2	Conclusion	48
6	Lithography	49
6.1	Introduction	49

6.1.1	E-Beam Lithography	49
6.1.2	AFM Lithography	51
6.1.3	Modification of AFM	51
6.1.4	Laser Assisted Beam Lithography	52
6.1.5	Future Direct AFM Writing	53
6.2	Conclusion	54
7	Testing Facility Modifications	55
7.1	Introduction	55
7.1.1	Thin Film Chip Mounting	55
7.1.2	Susceptibility and Four Point Probe	58
7.2	Conclusion	58
8	Overview of Results	59
	List of References	61
	Appendices	65
	Plasma Laser Deposition Procedure	66
	Chamber Preparation and Sample Mounting	66
	Pump Down Procedure	66
	Deposition Process	67
	Ending a Deposition Process	67
	Shutdown Procedure	68
	ICM Operating Procedures	69
	Chamber Preparation and Sample Mounting	69
	Starting a Deposition Process	70
	ICM Operation	70
	Ending a Deposition Process	71
	System Shutdown	71
	Ion Argon Mill Procedure	72
	Start Up Procedure	72
	Mounting Sample Into Mill	72
	Starting an Etch Process	73
	Sample Removal	74
	System Shutdown	74
	Photolithography	75
	Process Optimization	75
	Optimal Parameters For The SPR 700 Photoresist and MF24A Developer . .	75
	Laser Junction results	77
	Laser Junctions	77
	Technical Diagrams	83

List of Figures

1.1	A typical laser assisted molecular beam deposition system as given by M. Li <i>et al</i> [1]	5
1.2	AFM image of a typical YBCO pulsed laser deposition, showing micrometer particulates.	6
2.1	The figure shows a STBC laser beam characterization setup [2]	9
2.2	The figure shows an ideal laser profile [2]	10
2.3	The figure shows the ICM that was built to complement the PLD system .	10
2.4	Optimum ICM heat profile for YBCO thin film deposition	11
2.5	(a) XRD pattern of YBCO, (b) AFM surface scan, (c) Roughness of an ICM YBCO deposition at 2:1 oxygen to argon ratio at 30×10^{-2} mbar [3] .	11
2.6	Percentage susceptance against temperature graph of three YBCO layers. The blue graph is our 100nm YBCO reference film purchased from M.T.I. Corporation	12
2.7	Headway Research Inc. Model 1-EC101D-R485 spin coater	13
2.8	AFM picture (left) showing detail of a developed positive photoresist structure (right)	14
2.9	UV Suss mask aligner with additional new camera microscope for μm alignment purposes	14
2.10	Negative photoresist lift-off process where top and bottom films are separated	15
2.11	Ion argon mill mounted on common diffusion pump vacuum system	16
2.12	Pattern generated around an ultrasonically bonded gold wire can be clearly observed on a gold pad [4]	17
2.13	IV curve of a Josephson junction at 39K on 4th laser junction [4]	18
2.14	Shapiro step at a frequency of 9.073 GHz and 57.1K on 3rd laser junction [4]	18
2.15	Schematic representation of the device under test [3]	18
2.16	YBCO resistivity test setup of a Josephson junction test structure mounted to a PCB and cryogenic-cooler, also displayed is an AFM scan of 10th laser junction, at $3.1 \mu\text{m}$ [4]	19
3.1	Schematic diagram of a pulsed laser dDeposition system	20
3.2	Interferogram of a recorded laser pulse on a titanium target (left) and the simulated electron number densities (right) [5]	21
3.3	Plasma laser deposition system at Stellenbosch University	22
3.4	Plasma plume shown at various pressures ranging from 120 - 1200 mTorr and the effect on the surface roughness [6]	24
3.5	Effect of laser pulse repetition rates on quenched $\text{YBa}_2\text{Cu}_3\text{O}_{7-d}$ films [7] .	25

3.6	On the left is the rotating substrate holder with the cartridge heater. The right hand picture shows a release handle to position the heater and six temperature probes, with water cooling, to the substrate holder	27
3.7	Rotating substrate holder with shadow mask	27
3.8	Conversion from standard PLD chamber (right) to laser assisted molecular beam deposition (left)	28
3.9	Laser is focused into ablation chamber and atoms, clusters and ions are accelerated into vacuum via a supersonic jet (interchangeable)	28
3.10	PRCLA with shadow mask	29
3.11	Schematic representation of pulsed reactive crossed beam ablation	29
3.12	Stanford Research Systems DG535 digital delay timer (top) connects to pulsed valve driver (bottom) used to synchronize the gas pressure valve and the laser pulse for PRCLD	30
3.13	(A) Photograph of laser plume when gas valve and laser are triggered simultaneously; (B) Photograph illustrates a 2.2 ms pulse delay between gas valve and laser [8]	30
3.14	Delay pulses of the pulsed valve and the laser beam. [8]	31
3.15	YBCO PRCLA without (left) and with shadow mask (right) deposition done by de Villiers [8]	31
3.16	PLD droplet free zone described by Willmott <i>et al</i> [9]	32
4.1	Cylindrical target displaying magnetic poles and ion confinement and target erosion.	34
4.2	Rare earth button magnets are mounted between two mild steel rings in a copper cooling flange.	35
4.3	The water cooling pipes are insulated from the outer housing and vacuum tight.	35
4.4	Insert conversion from from ICM to planar sputtering.	36
4.5	New dual sputtering magnet configuration with improved target cooling	37
4.6	View of the completed dual sputtering head	37
4.7	Two of four different substrate heater types that were built for various applications.	38
4.8	Susceptibility tests for oxygen/argon ratios of (a) 1:2 (b) 1:1 (c) 2:1 and (d) 4:1 at a constant total pressure of 150 mTorr [3]	39
5.1	Diagram of the argon ion mill showing the chamber confining magnets surrounding the plasma chamber and the acceleration grids	42
5.2	Voltage potential across three grid ion extraction plates [3]	43
5.3	Plasma confinement diagram (left) and inside view (right) of actual plasma chamber with new acceleration grid	44
5.4	Multi cusp schematic with RF matching circuit [3] [10].	47
5.5	Fully adjustable substrate holder used to mill step etch profiles	47
5.6	RF shield designed around the argon ion mill	48
5.7	Gold plated glass slide showing a 10 min (30 mm diameter) and 5 min (22 mm diameter) ion beam etched area	48
6.1	Combination of optical and E-beam lithography with four alignment points as was done at University of Pennsylvania [11]	50
6.2	A 2 nm gap done by e-beam lithography and electron migration [11]	50

6.3	Multistage control box to control the x-y stage of the AFM.	51
6.4	The picture on the left shows the AFM scratch process, and on the right the actual YBCO constriction junction is shown [12].	52
6.5	AFM laser-etched constriction junction at 1,64 μm and a sub-micron constriction junction at 703 nm [4]	52
6.6	Self assembled growth of CNT-tip on conventional imaging AFM tip [13] .	53
6.7	AFM sulphur photolithography done by Germain <i>et al</i> [14]	53
7.1	Niobium superconductor chip holder with wire bonded IC constructed to shield the RSFQ circuit from external magnetic fields	56
7.2	Niobium superconductor RSFQ chip holder, attached to the 2.8 K cooling stage, with two temperature sensors A and B	56
7.3	New vacuum chamber mounted close to second stage cooling for minimum heat loss and improved noise reduction	57
7.4	Resistance plot indicating the superconductive transition, which only occurs with the shield on.	57
7.5	Measurements of an RSFQ test circuit with the compressor system switch off (left) and on (right)	57
7.6	High temperature cryogenic cooler with susceptibility and four point probe resistance measurement capability	58
1	First attempts at laser junction. Legs 1 and 2 were not successful	77
2	Laser junction leg 3 width measured 1.641 μm	78
3	Laser junction leg 3 (1.641 μm) Shapiro steps at 57.1K and 9.073 GHz . .	78
4	Laser junction leg 4 width measured 703.13 nm	79
5	Laser junction leg 4 IV curve at different temperatures	79
6	Laser junction leg 5 width measured 1.758 μm	80
7	Laser junction leg 6 width measured 1.523 μm	80
8	Laser junction leg 7 width measured 1.846 μm	81
9	Laser junction leg 8 width measured 1.875 μm	81
10	Laser junction leg 9 width measured 773,44 nm	82
11	Laser junction leg 10 width measured 3.125 μm	82
12	PLD eight substrate holder with single heater and temperature probe . . .	84
13	PLD eight substrate holder complete assembly detail	85
14	ICM component detail	86
15	ICM complete	87
16	Laser assisted molecular beam deposition detail	88
17	LAMBD chamber detail	89
18	LAMBD back main flange and substrate holder assembly	90
19	Complete ion argon mill main chamber assembly	91
20	Ion argon mill chamber and water cooled assembly detail	92
21	Argon ion mill flange detail	93
22	Argon ion mill electrode detail	94
23	Argon ion mill vacuum flange detail	95
24	Six substrate holder assembly detail	96
25	Six substrate holder main shaft and rotating handle design	97
26	Six substrate holder heater assembly design	98
27	Six substrate holder shield assembly design	99

28	Six substrate holder detail	100
29	Six substrate holder complete heater system detail	101
30	Six substrate holder vacuum chamber flange detail	102
31	Six substrate holder complete system assembly detail	103
32	Substrate heater design for 10 mm×10 mm substrate	104

List of Tables

4.1 Superconducting IV curves are shown with different oxygen to argon ratios obtained by ICM [3]	39
--	----

Nomenclature

A	Ampere
AFM	Atomic Force Microscope
CVD	Chemical Vapour Deposition
CeO	Cerium Oxide
CNT	Carbon Nano Tubes
DC	Direct Current
ΔT	Temperature Change
eV	Electron Volt
FIB	Focused Ion Beam
GHz	Giga Hertz
ICM	Inverted Cylindrical Magnetron sputtering
JJ	Josephson Junction
J_c	Critical Current
K	Kelvin
kV	Kilo Volt
kW	Kilo Watt
LAMBD	Laser Assisted Molecular Beam Deposition
LPCVD	Low Pressure Chemical Vapour Deposition
mBar	Milli Bar
mK	Milli Kelvin
MHz	Mega Hertz
MeV	Mega Electron Volt
MgO	Magnesium Oxide
MOCVD	Metal Organic Chemical Vapour Deposition
mTorr	Milli Torr
PLD	Plasma Laser Deposition
PRCLA	Pulsed Reactive Crossed Beam Laser Ablation
PECVD	Plasma Enhanced Chemical Vapour Deposition
RF	Radio Frequency
SEM	Scanning Electron Microscope
STM	Scanning Tunneling Microscope
SWCNT	Single Walled Carbon Nano Tubes
T_c	Critical Temperature
TiO ₂	Titanium Dioxide
TMP	Turbo Molecular Pump
UV	Ultra Violet
V	Volt
W	Watt
YBCO	Yttrium Barium Copper Oxide
ZnO	Zinc Oxide

Chapter 1

Foundations of Superconductor and Thin Film Fabrication

1.1 History

The discovery of thin films was a result of scientific research going back as far as the beginning of the previous century. Thomas Edison filed a US patent No: 767216 in the year 1903 on depositing metal on wax moulds using a cathodic sputtering process. Eight years later in 1911, H. Kamerlingh-Onnes, a Dutch physicist, unexpectedly discovered superconductivity while doing routine experiments. A member of his research group was purifying metals, and measuring their resistance as a function of temperature, while cooling down to 4 K. After experimenting with different metals, mercury was tested and at 5 K it suddenly showed no resistance. In disbelief this experiment was run a few times and eventually made public. In 1912 the first use of optical thin films for the production of mirrors was published by Pohl and Pringsheim [15]. Using a thermal evaporation technique, they vaporized metals, such as silver and aluminium, using magnesium oxide crucibles in high vacuum.

Thin films are usually denoted as atomic layers of a few hundred nanometers, which are produced in a vacuum system through evaporation or sputtering. While thin film technology was well on its way, Onnes dominated superconductor research until 1923, since at that time the laboratory in Leiden, Netherlands, held the only group that could make liquid helium. Thereafter a laboratory in Berlin and another in Toronto started, and in the early 1930s the Kharkov Physical Engineering Institute began research on low temperature superconductors. In 1933 W. Meissner and R. Ochsenfeld first discovered that the magnetic field in a superconductor is weakened to such an extent that it is forced out of the superconductor material. This became known as the Meissner effect. Thus, for a material to be a superconductor, two criteria would now have to apply, the loss of resistance and the expulsion of the magnetic field. Until then no theoretical explanation of the behaviour of a superconductor in a magnetic field had been given. By 1935, two German physicists residing in England, H. London and F. London, were able to formulate what is now known as the London equations.

In 1950 V. L. Ginzburg and L. D. Landau [16] wrote an article on a more general theory of superconductivity. Thereafter many groups focused on studying compound materials that could withstand strong magnetic fields and were able to conduct high current densities. By 1957 the actual mechanism of the superconductor effect was resolved by physicists J. Bardeen, L. Cooper and J.R. Schrieffer. In the BCS theorem, the phenomenon of an electron pairing which occurs in the superconductive state, also referred to as Cooper pairing, was described for the first time. A noteworthy experiment was conducted in 1960 by J. Kunzler and his research group. They demonstrated that a Nb₃Sn wire kept at a temperature of 4.2 K, in a magnetic field of 80 000 Oe, had a current density of 100 kA per cm². Such low temperature wires are also referred to as Type I superconductors and are still used to this day, in equipment such as NMR spectrometers. In 1962 an English physicist, B. Josephson, theoretically predicted an unusual electron tunneling effect, that would occur on superconductor contacts, also known as weak superconductivity or the Josephson effect. Up to then all the superconductors used were Type I and at low critical temperatures of below 10 K. Then came the major breakthrough in 1986, when two physicists K.A. Müller and G. Bednorz, working in Zürich, discovered a new type of superconductor, known as Type II or a high-temperature superconductor. This initiated a surge of interest and funding within many research groups across the globe during the years to follow [16]. Noteworthy achievements in superconductivity have been the superconductor quantum interference device (SQUID) that is able to measure femto-Tesla magnetic fields. Thus, in the medical industry these sensitive magnetometers could be used as a passive magnetic imaging system. It is interesting to note that the thin film and the superconductor discoveries happened within eight years of each other.

1.2 Thin Films

Thin film depositions are either purely chemical, in liquid-phase and gas-phase, or purely physical, as a solid material evaporative method. Many thin film deposition methods are used in the advanced micro-electronic device fabrication field in industry, which require complex and sophisticated approaches to fabricate sensors and devices. Methods used in chemical deposition are; chemical vapour deposition (CVD), low pressure CVD (LPCVD), plasma enhanced CVD (PECVD), atmospheric pressure CVD (APCVD), metal organic CVD (MOCVD) and thermal oxidation. Physical vapour deposition includes such methods as thermal evaporation, E-beam evaporation, plasma laser deposition (PLD), laser assisted molecular beam deposition (LAMBD), DC planar and inverted cylindrical magnetron (ICM) sputtering and RF sputtering.

Thin film depositions can also be complemented by using other techniques, such as spinning-on of organic materials to fabricate solar cells and using polymer based buffer layers in between thermally evaporated layers. When fabricating multilevel layers, positive or negative photoresists are used as a screen for etching, lift-off processes or when contact pads are required. Other fabrication steps may include electrolytic deposition, ion implantation, thermal oxidation, nitration, electroless metal deposition or silicide formation. Only methods currently used in our research group for the fabrication of superconductors, gas sensors and solar cells will be discussed.

1.2.1 Physical Sputter Deposition

The word "plasma" comes from the greek language meaning "something moulded or fabricated" [17]. To begin to understand the sputtering processes it is important to understand the fundamental plasma process. By definition "A plasma is a quasi neutral gas of charged and neutral particles which exhibits collective behavior." [17]. This means that, in a plasma, charged particles can move in local concentrations of positive and negative charges and generate currents and magnetic fields. These magnetic fields then influence other charged particles further away. Sputter deposition is a method where films are deposited with the aid of a plasma, as in the ICM. In many other techniques the plasma is a secondary feature used to produce ions, such as in ion beam sputtering. Here a particle strikes the surface with such energy that it dislodges atoms from the surface. The yield is defined as

$$Y = \frac{N_{ep}}{N_{ip}} \quad (1.2.1)$$

where N_{ep} is the number of emitted particles and N_{ip} the number of incident particles.

Sputtering occurs for virtually all incident species, such as ions, atoms, photons, electrons, molecules as well as neutrons and molecular ions. Thus sputtering uses ion bombardment of inert gas ions such as Kr^+ and Ar^+ , or even small molecular ions such as O_2^+ and N_2^+ .

Physical sputtering is the transfer of kinetic energy and physical momentum of the incident particle to the atoms at the surface. This is independent of the particle's charge. The incident particle or ion impacts the surface of the solid material, or target with sufficient energy to dislodge atoms by breaking their bonds. During this process, atoms are removed from the solid and are considered to be sputtered atoms.

1.2.2 Sputter Energy Dependence

Physical sputtering ranges from energies near the binding energy, to many MeV. At low energies, with incident ion energies of a few eV up to 30-40 eV, there is little to no sputtering. It is generally thought that the minimum ion sputter energy is the weakest binding energy of the surface atoms to one another. The yield at this energy level is normally below 10^{-2} in the 30-40 eV range, and rapidly declines at lower ion energies to a level of 10^{-6} and below.

The knock-on energy regime is at energy levels of 40 to 1000 eV. Here, the incoming particle has enough energy to dislodge many hundreds of atoms. After the first collision the incident particle, together with the impacted atom, move on into the material, causing multiple collisions. The yield for individual collisions can vary from 0 to 10 or more atoms. The average collision rate is characterized by the thin film deposition process's sputter yield.

Knock-on sputtering describes the practical energy range used for many sputtering systems. The rate at which sputtering or sputter deposition takes place is a roughly linear function with respect to the input power that is applied. At higher ion energies, 1 keV to 50 keV, the incident ion or particle will have enough energy to dislodge atomic bonds in a spherical area around the impact site. Even though this region allows for a much higher yield than with the knock-on regime, it is impractical for industrial scaled purposes due to the high voltages and power levels required. At higher energies, above 50 keV, the particle will have enough energy to penetrate the surface substantially before stopping and releasing its kinetic energy. There is little or no damage at the surface of the bulk material and most of the damage is at about a micrometer below the surface. Thus, the incident particle will now be implanted, depending on the energy applied. To sputter ions, two methods are used; namely, ion beams and plasmas.

The difference is that in a plasma source, the target surface to be bombarded is positioned in the plasma, while in the case of the ion beam, the target is separated from the plasma and ions are extracted from an ion source and then directed to the target surface from which atoms are sputtered.

1.2.3 Pulsed Laser Deposition

Pulsed laser deposition also falls into the category of physical sputter depositions. It consists of a laser, vacuum chamber, turbo molecular pumps, roughing pump, water cooling system, vacuum pressure sensors, rotating target holder, heated substrate holder, gas inlet valve system and two focusing optical lenses to focus the laser beam.

A laser beam is focused into a vacuum chamber, striking a target at a 45° angle. The vaporized atoms create a plasma plume. The energy of the plasma is directly related to the laser energy or fluence. Two viewing ports are located so that the plasma plume may be seen perpendicular from the top and the side for alignment purposes. For reactive reactions a partial pressure of gas, such as oxygen, is introduced to the chamber. The atoms collide with the gas and are accelerated toward the substrate, where it then deposits under heated conditions. This has become a very versatile tool, since any solid or molten material ablated will take on the stoichiometric structure of an existing structure and gases can be added to react with the plasma to form new materials.

In our research group PLD is used specifically to produce high-temperature superconductors using yttrium barium copper oxide (YBCO). Almost all materials that can be placed under vacuum without evaporating can be used for thin film deposition. Due to the excessive cost of this instrument, the vacuum system peripherals, and the fact that the fabrication of any device is very time consuming, this process is not cost effective for industrial fabrication purposes.

Laser ablation used in a different setup, where the laser is pulsed into a tube furnace, can also be used to generate single walled carbon nanotubes (SWCNT), using the Smalley Process [18].

1.2.4 Laser Assisted Molecular Beam Deposition

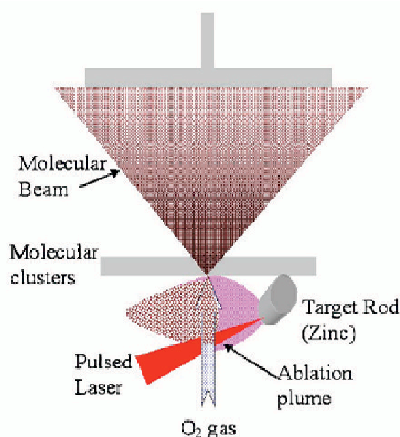


Figure 1.1: A typical laser assisted molecular beam deposition system as given by M. Li *et al* [1]

Laser assisted molecular beam deposition is a derivation of the plasma laser deposition system and has the added capability of generating high energy source particles and a high quality film growth at lower substrate temperatures [19]. The target is separated in its own chamber and the plasma plume can be in pressures of up to 2 or more atmospheres, which is not possible with the standard PLD system. The laser beam is pulsed through a quartz window into the target chamber, striking the target, as shown in Fig. 1.1.

A reactive gas, such as oxygen is pulsed and can be suitably adjusted so that the reactive molecular ratios are met, allowing it to react with titanium to form TiO_2 or with other materials such halides, Si, C, metal oxides and metals. The gas pulses are timed so that the laser and the gas pressure are synchronized. The clusters generated then pass through a supersonic jet into the vacuum chamber, where the substrate is heated and rotated. Growing YBCO should also be possible, as shown by DeLeon *et al* [20] and this gives us another method to create simpler clusters as well, which will most definitely be of use to our research group in the future.

1.2.5 Chemical Vapour Deposition

CVD is the formation of thin film solids by decomposing gaseous chemicals using plasma, heat, ultraviolet light or a combination of different energy sources. CVD is mostly used in the semiconductor industry to dope either n-type or p-type silicon wafers. Our research group is currently focusing on gas and pressure sensing devices, where CNTs and ZnO nanorods are grown on a catalyst using a CVD system. This electric furnace has a 1 meter long quartz tube with a diameter of 25 mm.

The quartz tube can be used in temperatures as high as 1200°C . On either side of the tube a vacuum tight connector is fitted which connects to the gas feed on one side and

on the other to an outlet, through which gases are bubbled into water and extracted away. The bubbler is normally positioned further away from the furnace to allow for the hot gas to cool down. A temperature controller is linked to a computer and has the capability of setting eight different temperature profiles. In addition to the system there are two flow meters to control the reaction rates for the correct growth rate.

Other applications, such as the annealing in oxygen of, for example, YBCO, CeO and ZnO powders and pressed pellets can be re-annealed to form the targets in the PLD system. As briefly mentioned, there are many variations of the standard CVD process. However, these methods are currently not being used by this research group.

1.3 Conclusion

It will be shown that it is possible to execute most of these techniques by using the existing equipment and not incur high expenses. From the original PLD system, additions and modifications were made to incorporate PRCLA and LAMBDA. Thus, from a simple system, a more complex and versatile system was created.

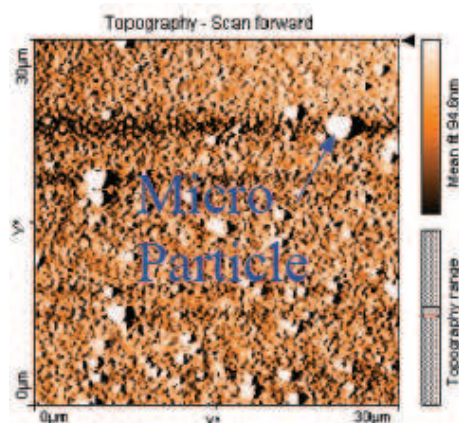


Figure 1.2: AFM image of a typical YBCO pulsed laser deposition, showing micrometer particulates.

The PLD system is very versatile and it is possible to deposit insulating and conductive materials. The main problem is that laser droplets or particulates are formed at the target and deposited on the substrate surface, as shown in Fig. 1.2. These particulates are of micrometer size, whereas the general surface has a roughness of approximately 30 nm.

The building of an independent DC inverted cylindrical magnetron system gave our research team the freedom of using both PLD and an off-axis sputter system. Comparisons of the quality of the thin films could now be investigated.

Chapter 2 will cover device fabrication and show a step by step methodology, including the testing procedure, to determine the quality of the layers produced and then, once the device has been completed, the testing of such a sensor.

Chapter 3 will concentrate on the PLD system and a possible solution to the micro particulates produced. A new design will be shown and all the modifications that were made to make the system more versatile will be described.

Chapter 4 will describe the ICM sputter system design and how this was adapted to the existing vacuum system, as well as the results obtained in making a 150 nm thin film superconductive layer.

Chapter 5 will focus on building an argon ion mill and on further modifications made to the system to realize an even and uniform beam that can be used to etch our thin films.

Chapter 6 will concentrate on lithography methods and new trends, and also show modifications made to the AFM to allow for nanolithography scratching over a large area, and modifications done to measure the piezo-electric effect of ZnO nanorods.

Chapter 7 will highlight modifications done on the low and high temperature cryogenic test facilities and conclude with the prediction of what can be done in the future to enhance the capabilities of the research group. In creating new devices, innovative ideas are needed to allow for atomic scale resolutions to become seen and controlled.

Chapter 8 will give an overview of the results obtained and suggest future ideas and possible modifications to equipment.

Chapter 2

YBCO Device Fabrication Process

2.1 Introduction

The fabrication process of a superconductive Josephson junction device will be outlined and an overview of the whole fabrication process, available at the Electrical and Electronic Engineering Department, will be shown. Plasma laser deposition had been the only method available, until the ICM was developed for the deposition of YBCO thin films. The device fabrication method used is considered to be top-down, where materials are first deposited and then etched away using a lithography process.

Magnesium oxide (100) has primarily been chosen as a substrate for the YBCO thin film deposition process, due to its low dielectric losses, which makes it ideal for high frequency microwave applications and devices. The substrate is cleaned and then a thin film of YBCO is deposited by PLD or DC sputtering. Photoresist is used as a protective coating, while the substrate is being cryogenically cooled and tested. After the thin film has complied with certain conditions the next process can start. A UV lithography process follows and the device is patterned.

The sample is now ready to be etched. There are two etching processes available; either chemical wet etching or a dry argon ion mill etching process. After etching, a mechanical copper mask is used as a template to deposit contact pads. Silver or gold pads are either thermally evaporated or deposited with the PLD system. The next step is to mount the device onto a printed circuit board and wire bond the pads to the copper tracks of the board. Now the device can be cooled down to the superconductive state and tested.

2.1.1 Substrate Choice and Preparation

The magnesium oxide substrate chosen has a crystal orientation of (100) and a mismatch of 8.8 %, to the lattice structure of the orthorhombic crystal structure of YBCO. Due to the imperfect match, the YBCO lattice is strained within the first few atomic

layers, but then aligns itself correctly thereafter. It is important to grow the correct structure and in our case we are interested in a crystallographic c -axis growth. This axis is perpendicular to the substrate and is ideal for device fabrication, due the mobile electrons being in a plane parallel to the surface. The deposition temperature plays an important part in the formation of a -axis or c -axis crystal structures. Lower temperatures favor a -axis growth. Even though a single crystal substrate is used, twin boundaries of a and b axes could exist within the c -axis orthorhombic structure. Disorientated lattice matching could also occur between island growths, known as can threading dislocations. The surface roughness plays an important part in the reproducibility of designed circuits. The lower the surface roughness, the fewer defects, such as columnar growths, shadowing, strain, voids and volumetric changes, are present. The MgO substrates purchased have been pre-cleaned and can be used as is. If, however, the substrate has been used before, then it would be necessary start by polishing the sample via a chemical mechanical method developed by Kang *et al* [21].

The method mentioned entails making up a mixture of 2 vol % phosphoric acid (H_3PO_4) and 10-20 nm colloidal silica particles, and polishing the MgO substrate with this slurry. It was shown that using this method makes it unnecessary to anneal the substrate at high temperatures.

2.1.2 Thin Film Deposition

There are two physical deposition systems available to our group; pulsed laser deposition (PLD) and thermal evaporation. The inverted cylindrical magnetron sputtering (ICM) was designed and built as a third option. The PLD system is one of the most versatile methods used in thin film deposition systems, due to the high energy levels of the plasma, which also contributes to better adhesion and mobility of the atoms on impact. A further advantage is that the target material used can be either an insulator or a conductive material. Once the YBCO layer, 150 nm thick on average, has been deposited, the surface roughness is determined. Each superconductor has a minimum critical thickness, as shown by A. Abert *et al* [22].

Unfortunately our excimer laser beam profile is not uniform and has low and high energy domains within its beam. This leads to clustering, and deposition of large molten particles, as discussed later in this chapter.

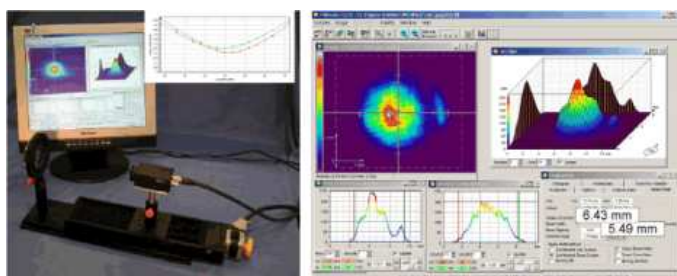


Figure 2.1: The figure shows a STBC laser beam characterization setup [2]

In Fig. 2.1 we see a typical excimer energy profile of a focused laser beam. Ideally we would like to optically shape the laser to have a uniform energy profile, as seen in Fig. 2.2. For this a homogenizer would be suitable to transform the energy peaks and create an even energy distribution.

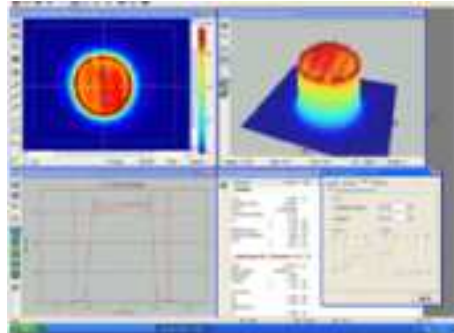


Figure 2.2: The figure shows an ideal laser profile [2]

Purchasing a homogenizer would have solved our problem. However, due to financial constraints it has not been possible.

Although the YBCO thin films show a high critical temperature (T_c) of 91K, the surface roughness is in the region of 32 nm, with intermittent micrometer particulates on the surface. When patterning Josephson junctions, these micro particulate structures influence the success rate of the device fabrication process. Following these shortfalls, and the limited accessibility of the PLD system, which was used by three different research groups, the necessity to develop an alternative method was investigated.

The investigations led to the design of an off-axis type of DC sputtering method, also known as an inverted cylindrical magnetron (ICM), being developed for the superconductor group as shown in Fig. 2.3. The thin film layers produced, show a 5-10 nm roughness, as shown in van Staden's thesis [3]. Although this method is ideal for YBCO thin film deposition, it is limited to conductive targets. A lithography process before YBCO growth is not possible, due to the high temperatures during thin film growth.

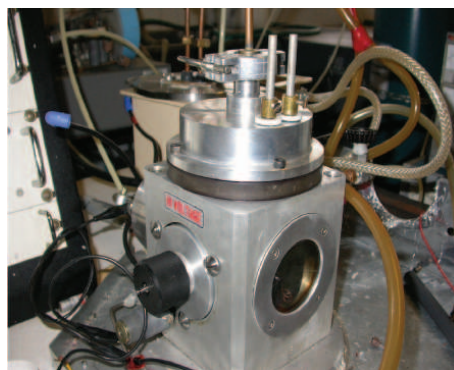


Figure 2.3: The figure shows the ICM that was built to complement the PLD system

Since the substrate is connected via silver paste to the heater, there is always some difficulty removing the substrate after the deposition process. This led to some of the

substrates being damaged. Changes were thus made, and a heater system was designed and built to allow the substrate to be heated without using silver paste.

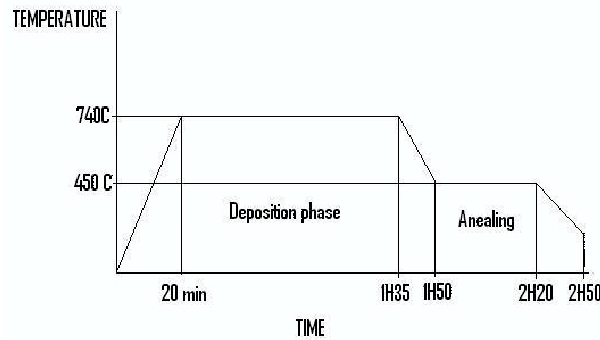


Figure 2.4: Optimum ICM heat profile for YBCO thin film deposition

DC sputtering is done following the optimum pressure and heat profile parameters set by van Staden [3], shown in Fig. 2.4. Following this pressure and temperature profile, a T_c of 89 K was achieved.

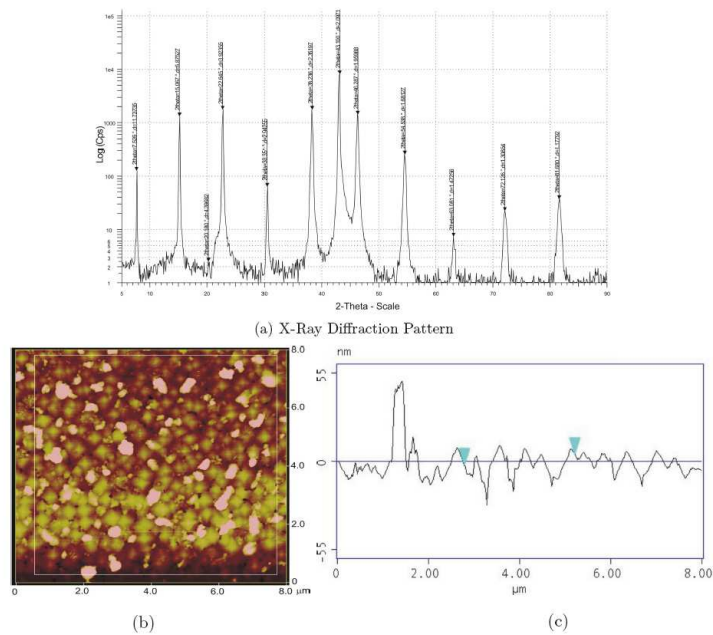


Figure 2.5: (a) XRD pattern of YBCO, (b) AFM surface scan, (c) Roughness of an ICM YBCO deposition at 2:1 oxygen to argon ratio at 30×10^{-2} mbar [3]

The best surface roughness parameters were obtained by van Staden [3] and are represented in Fig. 2.5((b), (c)), at 4 nm. The X-ray diffraction scans illustrated in 2.5(a), show well defined (001) peaks, which correspond to orthorhombic YBCO. Following the procedure in Appendix B, optimal sputtering conditions are given to achieve the deposition shown above. Susceptibility of the YBCO thin film layer was also tested and quantified.

2.1.3 Analysis of Thin Films

In order to test the quality of a deposited YBCO thin film, a susceptibility test is done. This test is based on the Meissner effect, where all magnetic flux is expelled from a superconducting film once the film goes into the superconductivity state. The data received from the pickup coil is represented by a percentage signal, versus the temperature of the YBCO substrate. A graph depicting this information is reproduced in Fig. 2.6.

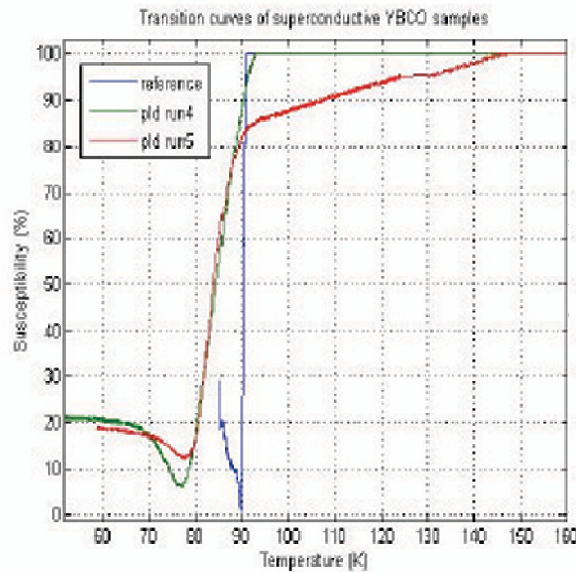


Figure 2.6: Percentage susceptance against temperature graph of three YBCO layers. The blue graph is our 100nm YBCO reference film purchased from M.T.I. Corporation

With this information it is possible to analyze the uniformity and quality of the YBCO layer. The graph shows two measurements done on thin films deposited in the ICM compared to a purchased reference thin film. The uniformity of the layer is related to the sharpness of the transition ΔT to the superconductivity state.

2.1.4 Spin Coating

The clean substrate is coated with photoresist on a spin coater as shown in Fig. 2.7. Lithography parameters are very specific to the photoresist and, as indicated on the data sheet, will have different process parameters. As the YBCO thin film has a different etch ratio to the photoresist when dry etching, a ratio of 1:10 to the YBCO film thickness and the photoresist thickness is kept. If a lift-off process is needed, then a negative resist is preferable, since it undercuts and allows for easy lift off. A very popular resist is the AZ5214E, which has the ability to be either a positive or a negative resist, and which is suitable for ion argon milling.

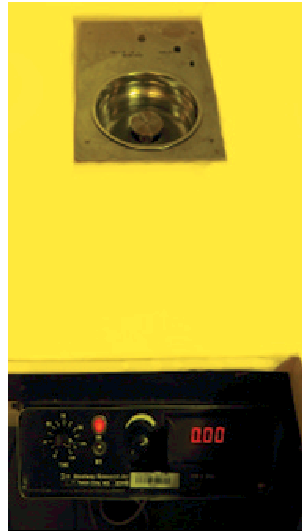


Figure 2.7: Headway Research Inc. Model 1-EC101D-R485 spin coater

A volatile type of photoresist is used, which unfortunately creates an edge bead after the spin process. It is important to keep the edge bead as low as possible, to allow for substrate and mask distance to be kept to a minimum and prevent diffraction errors.

2.1.5 Soft-Baking

After spin coating the substrate is soft-baked. This will dry out the volatile solvents in the photoresist and prevent the substrate from contaminating the mask. Any thermal shock should be prevented, as this will cause cracking on the surface of the photoresist. The photocatalytic properties of the photoresist must be retained and over-baking would affect the sensitivity, and also the repeatability.

2.1.6 Optical Ultra Violet Photolithography

The photosensitive polymer is exposed by a UV source through a mask. As the polymer structure is then altered, bonds are either broken by the exposure to the UV source or strengthened, depending on the type of photoresist (positive or negative). In photolithography it is very important to make sure that there is no air gap between the mask and the substrate and that the chrome side of the mask faces the substrate so that no diffraction errors are introduced. After exposing the photoresist it is then developed and, again, the timing and temperature is important when working with very fine structures. To create reproducible results, all the parameters must be the same, such as spin coater speed, temperature and time of development.

After development, the critical dimensions are viewed with the AFM, as shown in Fig. 2.8, to quantify the angle and height of the photoresist and to measure the critical dimensions to check that they are correct.

After development of the photoresist the substrate has to be post-baked to prepare the layer for ion- or chemical etching. This is done at a lower temperature to allow for all solvents to escape and the photoresist to harden. The temperature is kept low so that there are no sagging effects which could compromise the dimensions.

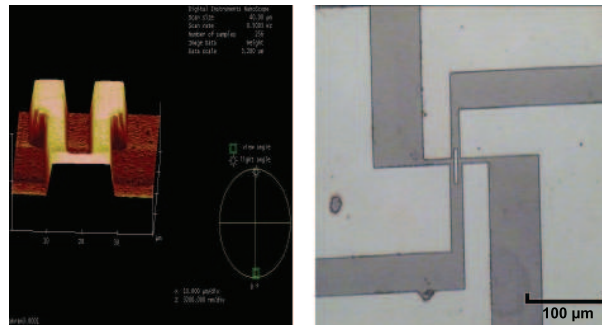


Figure 2.8: AFM picture (left) showing detail of a developed positive photoresist structure (right)

A further modification was made to the mask aligner, to allow for fine resolution alignment of structures down to $2\ \mu\text{m}$. This is especially important for bi-crystal alignment. The light reflector lens that fits into the tube system of the microscope, is fitted with an infrared coaxial LED light. The light frequency was chosen to be in the red spectrum so as not to develop the photo resist before UV exposure. This was documented by Graser [23]. The modified mask aligner is shown in Fig. 2.9.

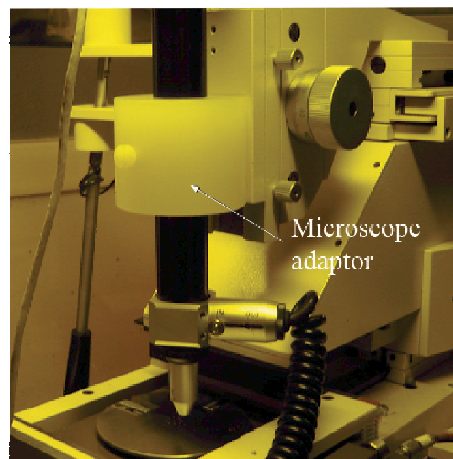


Figure 2.9: UV Suss mask aligner with additional new camera microscope for μm alignment purposes

2.1.7 Photoresist Developing

Once the positive photoresist has been UV exposed, it is submersed in developer for a certain time, at a certain temperature. Then the substrate is rinsed in deionized water and dried in nitrogen gas. Modifications were also done to the existing microscope to improve resolution, and the white spectrum LED was replaced by a red LED, to prevent

any further exposure. If the edges are underdeveloped, the layer can be developed further until the correct results are achieved.

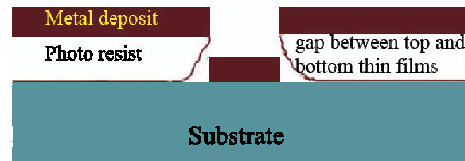


Figure 2.10: Negative photoresist lift-off process where top and bottom films are separated

Negative resist is used in lift-off processes. Due to the light refraction pattern passing through the chrome mask, an undercut is created. Once developed, an overhang is created, which is ideal for lift-off processes. In Fig. 2.10, one can clearly see that the top of the metal layer is not connected to the deposited layer.

2.1.8 Post-Baking

Post-baking hardens the photoresist further and is done at lower temperatures, without changing the critical dimensions of the patterned resist. This is a prerequisite, again specified by the supplier, to prepare the photoresist for dry-etching. Using higher temperatures creates sagging or deformation of the structure.

2.1.9 Chemical Wet Etching

Chemical etching of YBCO is done with a 10% concentration of citric acid and deionized water solution. If there are very fine structures, this method is not ideal, since chemical undercutting occurs and etches through these fine structures. Also, the edges are left jagged and junctions are not reproducible [24]. This inability to reproduce consistent dimensions under $10\mu\text{m}$ led to the investigation into dry ion argon etching or milling.

2.1.10 Argon Ion Milling

Argon ion milling occurs when argon gas ions or positively charged atoms are accelerated, forming a beam of energetic particles and causing removal of the material in its path. The energies are controllable, but cause heating of the etched surface. This may lead to the degradation of the superconductor. Possible remedies are to cool the substrate with liquid nitrogen [25], or to expose the etched surface to controlled bursts of energy by adding a slotted rotating disc into the chamber.

The argon ion mill was based on a previous design [26]. It was adapted to fit onto the existing vacuum system, and further modifications were done to the water cooling and acceleration grids to finally create a working mill with a broad beam of 30 mm, as described later in Chapter 5. Prior to the etching process, the sidewall profiles were

measured by using an AFM for the optimization of the lithography process. When considering ion milling, the angle of the photoresist to substrate is important, since this will influence the milled edges of the thin films. As the photoresist mills faster than the YBCO, the angle of the resist will cause a gradient on the YBCO thin film. This is an especially important consideration when creating step-edge Josephson junctions. Fig. 2.11 shows the Argon Ion Mill and the modifications made to fit onto an existing diffusion pumping system.

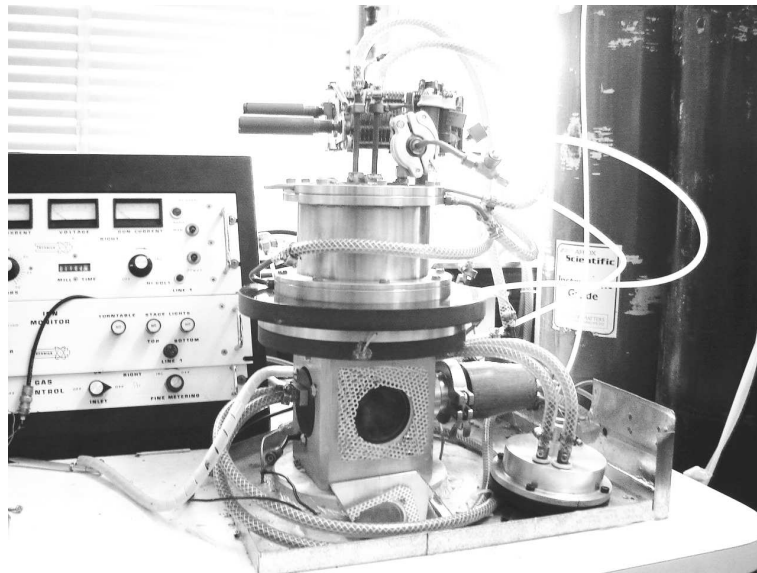


Figure 2.11: Ion argon mill mounted on common diffusion pump vacuum system

After the patterning has been realized, the substrate is mounted on the water cooled sample holder and the sample is ready for milling. Cooling the substrate is important, due to the high level of ion energy striking the polymer photoresist. First the base pressure must be reached before the argon gas is set to the correct pressure. The RF supply is switched on and brought into resonance by adjusting the capacitance. Once the plasma is on, the argon pressure is set to 2×10^{-4} mbar and the reflected energy is set to a minimum by adjusting the capacitance again.

There are three grids: positive, earth and negative. If the acceleration voltage is too high, oxygen depletion occurs in the YBCO thin film. This can be reversed by doing a post-anneal later. However, in the worst case, irreversible ion damage to the YBCO crystal lattices will occur on the fine structures.

When creating step edges, higher voltages can be used, but this requires sufficient cooling of the photoresist. After milling, the photoresist can be removed by rinsing the substrate in acetone or using a photoresist stripper. If, however, the ion energy has damaged and carbonized the polymer structure through overheating, removal may be impossible.

One method for overcoming the heating effect is to mill for shorter times, allowing the substrate to cool down. Also, establishing a good heat transfer by using thermal heat sink paste improves the heat conductance while milling.

2.1.11 Contact Pads

A copper mask with 0.5 mm holes is used, and alignment is done under a microscope. For more complex structures the lithography process will have to be repeated, and the next process would have to be aligned onto the previous layer. Once all the layers have been completed, the contact pads have to be deposited. The methods we have available for the deposition of gold or silver pads are PLD, sputter deposition and thermal evaporation. A Cr or Ti buffer layer of around 8nm is used for gold and silver adhesion.

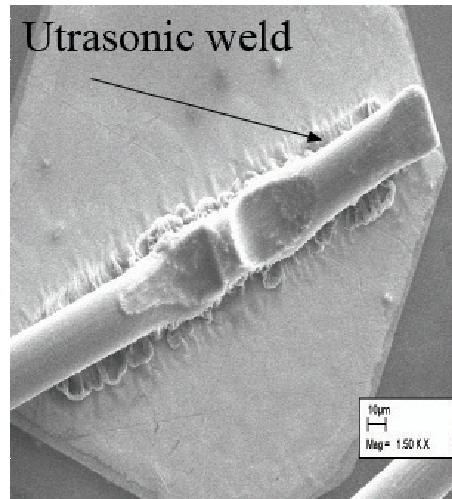


Figure 2.12: Pattern generated around an ultrasonically bonded gold wire can be clearly observed on a gold pad [4]

The minimum deposition thickness of silver or gold is about 360 nm when using our ultrasonic wire bonder. In the SEM Fig. 2.12 one can clearly see how the ultrasonic vibrations, created by the wire bonding system, have lodged the wire onto the gold pad. After deposition of the contact pads the device is glued onto a PCB and wire-bonded. Then it undergoes a resistivity test, where the voltage is measured under a constant current. The IV curve of each junction is also measured at a chosen temperature below T_c .

2.1.12 Testing the Superconductor Device

After completion of the fabrication process the Josephson junction (JJ) can be tested. This is done in a four point probe configuration across the JJs. An IV curve taken at a junction temperature of 39 K is shown in Fig. 2.13.

A high frequency sweep between 2-18 GHz is fed to an antenna positioned above Josephson junctions (Fig. 2.14). With this high frequency antenna it is possible to induce a critical current into the junction and produce Shapiro-steps. It can clearly be seen that the currents induced at certain frequencies create a temporary loss in superconductivity.

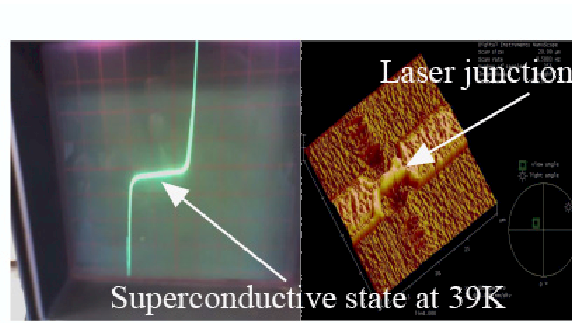


Figure 2.13: IV curve of a Josephson junction at 39K on 4th laser junction [4]

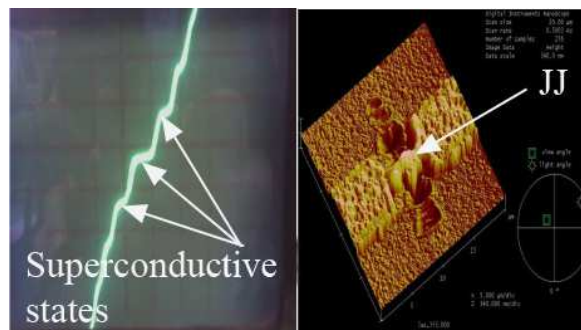


Figure 2.14: Shapiro step at a frequency of 9.073 GHz and 57.1K on 3rd laser junction [4]

A block diagram of the test setup is shown in Fig. 2.15 [3]. Once all the Josephson junctions have been tested and quantified, comparative checks are made and this is an indication of the repeatability of the construction of each of the junctions.

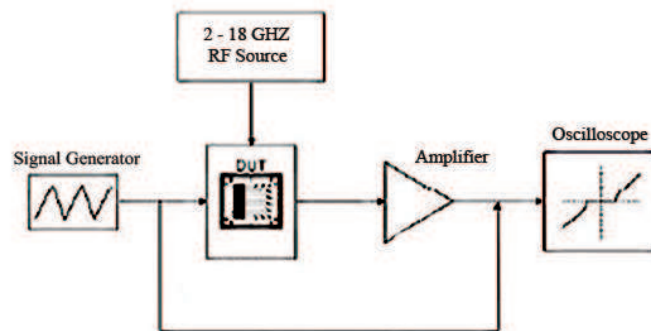


Figure 2.15: Schematic representation of the device under test [3]

Fig. 2.16 shows the cryogenic test facility used to measure the thin films and the tunneling currents of the superconductive thin films and devices.

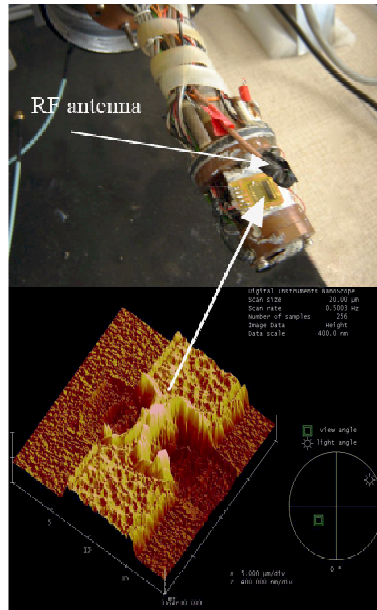


Figure 2.16: YBCO resistivity test setup of a Josephson junction test structure mounted to a PCB and cryogenic-cooler, also displayed is an AFM scan of 10th laser junction, at $3.1 \mu\text{m}$ [4]

2.2 Conclusion

When constructing Josephson junctions, the bi-crystal junctions are the most widely used and most reproducible. We have explored alternative methods in creating Josephson junctions, due to the high costs of bi-crystal substrates. So far buffer step-edge junctions were made by van Staden [3], CeO bi-epitaxial junctions were done by de Villiers [8], AFM nano-ploughed junctions by Elkaseh [12] and laser constriction and tunneling junctions were also done by the researcher [4]. The laser junctions have been successfully fabricated and further results will be given. Even though this has been accomplished, reproducibility of identical Josephson junctions is still a difficult task to master.

Chapter 3

Pulsed Laser Deposition

3.1 Introduction

The existing plasma chamber was designed and built in 1995 by The National Accelerator Centre. This 308nm laser is a XeCl Lambda Physik EMG 203 MSC which produces 300 mJ for each 25 ns pulse. The maximum pulse repetition rate is 100 Hz, however, it is mostly used at between 1-20 Hz. The intensity of the laser can be varied by changing the input voltage of the laser from 18 kV to 25 kV. Fig. 3.1 shows a schematic diagram of a PLD system.

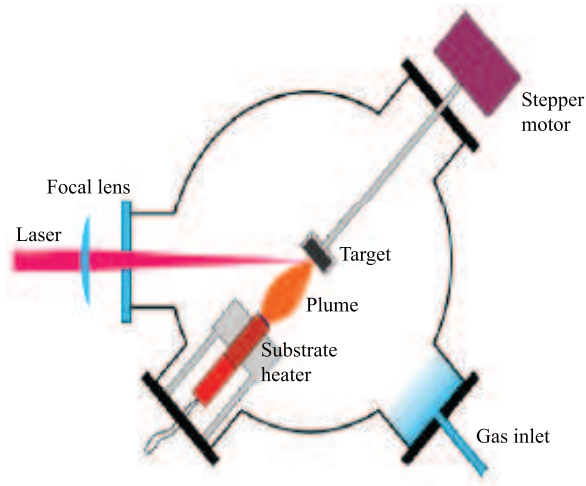


Figure 3.1: Schematic diagram of a pulsed laser dDeposition system

The total surface area of the laser is measured at the output of the laser source. The laser beam is first reflected via a mirror toward a set of focusing lenses. Here, the beam is focused by a set of spherical adjustable silica lenses into the vacuum chamber and strikes the rotating target at a 45° angle. Once focused on the target, the energy per pulse can be calculated. The high-powered excimer laser pulse then evaporates the target material and behaves like a shock wave, as shown in Fig. 3.2 [5]. This is also known as a plume. In PLD the target bulk material is ablated, such that the symmetry

of the materials or atomic bonds are preserved and stoichiometric growth is preserved. While the target is ablated, it is rotated so that the damage is limited to the surface track being evenly eroded. As the laser strikes the target, highly energetic particles (plume) are ejected normal to the target surface. These particles include bulk molten target material, ions, clusters, oxide molecules and atoms. The plume expands away from the target with a strong forward-directed velocity of approximately 10^6 cm/s and a distribution of the different particles can be as many as 10^{19} species/cm per pulse. It has been shown by Koren *et al* [27], that lower wavelength ablations have better surface roughness and uniformity when depositing thin films.

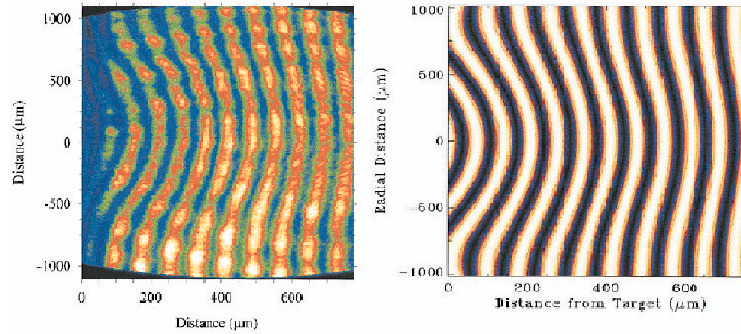


Figure 3.2: Interferogram of a recorded laser pulse on a titanium target (left) and the simulated electron number densities (right) [5]

The ablated species condense on the substrate placed opposite to the target, which is heated to a certain temperature to ensure proper stoichiometric growth onto the crystal structure of the substrate. This chapter explains the general procedure and parameters being used, followed by a brief discussion on the effects of each parameter, then showing solutions that were introduced by other research groups reducing the contamination of the surface by particulates.

3.1.1 Experiment Parameters

The ablation process takes place in a vacuum chamber with single or multiple reactant background gases. In the case of gold or single element depositions, no gases are present. In the case of oxide films, oxygen is used as the background gas. For example, the oxygen pressure for YBCO thin films is approximately 0.2 - 0.005 mbar. In addition, the substrate temperature has to be sufficiently high (700°C - 800°C) and uniform across the whole substrate area to obtain epitaxial films. Laser-pulse energy density on the target should also be greater than a certain threshold value (for YBCO, $1 \text{ J}/\text{cm}^2$).

For device fabrication, the film thickness is typically 100 - 200 nm for YBCO thin films. If the deposition rate is 0.1 nm/pulse, then 1 - 2 thousand laser pulses are required for the experiment. The uniform film area is determined by the dimensions of the central part of the plume. The substrate being used is 1 cm^2 . The area can be increased either by scanning the laser spot across the target, or by scanning the plume

across the substrate, by moving the substrate relative to the plume or by increasing the target-substrate distance.



Figure 3.3: Plasma laser deposition system at Stellenbosch University

3.1.2 Chamber Considerations

As many users are working on the PLD system, cross contamination could occur from one experiment to another. It is good practice to have numerous chambers, each of which is dedicated to certain oxidative or purely metal type experiments. This, however, becomes very expensive. Not wearing gloves also introduces contamination, causing degassing to occur under vacuum, which prolongs pumping down times. Flushing the chamber with nitrogen before opening will also prevent contamination by water vapour. Moisture seems to affect the quality of the YBCO growth [28].

If, however, there is only one chamber, then a good practice would be for each user to have their own thin metal insert, made of either aluminium or stainless steel. This would allow them to cover the inner chamber and protect it against contamination. Experiments that are using different target types could then be run in the same chamber.

3.1.3 Target

The target disc contains 99.999 % pure YBCO bulk (123) material, is sintered at about 930°C (which is the standard procedure to reach the superconductive phase) and is

pressed into a pellet. Recently studies on the particulate size and the elimination of a -axis growth in thick 650nm c -axis orientated thin films have been published by Zhu *et al* [29]. Experiments were done, changing the annealing temperature when fabricating the target.

Two important findings were made; firstly the grain sizes were in the range of ten micron to submicron size when annealed at 930°C. When ablated these would create particulates, where clusters of a -axis oriented molecules would sit on the surface and would not integrate into the heated thin film layer. Secondly, when a non-superconducting phase is formed under sinter temperatures of 800°C, the grain size created is smaller than 20 nm. Thus, when ablated, the nano-particulates would be able to be absorbed into the layer, preventing a -axis growth in thicker layers above the critical thickness. For more information on the standard target preparation, refer to the thesis of Graser [23].

3.1.4 Laser Density

The laser energy density, or fluence, can be set using a pyro-electric detector. By determining the initial laser area and the focused laser spot size the fluence can be calculated. The focused laser is pulsed (to make sure the pulsed energy is at its peak) onto thermally sensitive fax paper or black plastic film (negative). The threshold energy density of YBCO is 1 J/cm² [30]. The ideal energy density used in YBCO deposition is 2.6 J/cm [31]. It is important to note that the beam profile, the target preparation [29], as well as the pressure and substrate temperature, determine the quality and roughness of the thin film.

If the laser profile is non-uniform there will be low and high intensity fields in the focal spot, which will contribute to clustering of the target material on the substrate, causing it to become rougher. The use of an homogenizer will greatly improve the laser quality.

3.1.5 Base Pressure

A good base pressure will allow fewer contaminants mixing with the reactive gas during the deposition process and ensure reliable results being attained. Ideally, in our PLD chamber, a vacuum of 3×10^{-6} mBar should be reached, if pumped overnight.

For routine experiments, where oxides are being used, a 2×10^{-5} mbar pressure is acceptable for the experiment to continue. Research done by Kuriki *et al* [28] showed that degassing to a pressure of 3 to 1×10^{-6} had a positive effect on the current density (J_c) if the chamber was heated externally, with a heater band, for 2 to 5 hours whilst vacuuming. It is explained that water molecules diffuse into the YBCO and affect the oxygen vacancies within the CuO basal plane [32], and this then leads to the eventual decomposition of YBCO [33].

3.1.6 Gas Pressure

The gas pressure is a critical setting that determines the quality of the YBCO, as it directly influences the plume size and deposition uniformity. A comprehensive study was done by Haugen *et al* [6]. In the pictures below there is a clear change in the plume size with the change in pressure and the orange-red colour is an indication of the oxygen reaction taking place. As the chemical species and ionic ratios change, the surface quality changes, as seen below in Fig. 3.4.

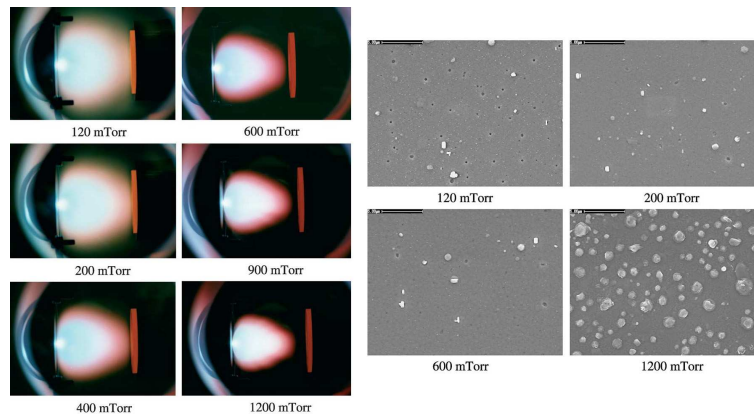


Figure 3.4: Plasma plume shown at various pressures ranging from 120 - 1200 mTorr and the effect on the surface roughness [6]

3.1.7 Target To Substrate Distance

The critical distance to target has been defined by Lopez *et al* [7] where the plume length is defined as L and $1.2 \times L$ is the optimal distance the substrate is to be positioned from the target. Experiments done by Haugen *et al* [6] also confirm this distance and in addition, have been able to prove that $0.8 \times L$ and $1.2 \times L$ seem to be the optimal distances. The plume is also dependent on the oxygen gas pressure and so the optimal distance has to be chosen based on the deposition pressure.

3.1.8 Pulse Repetition Rate

Currently the pulse repetition rate is set at 10 Hz. Studies done by Lopez *et al* [7] on the effect of changing the pulse rate show that the rate could possibly be optimized at a rate higher than 10 Hz. From the graph, Fig. 3.5, it can be seen that a higher laser pulse repetition rate on quenched YBCO improves the T_c . Further studies are needed to determine the upper limits. Always pre-ablate to clean the surface of any contaminants, before exposing the plume to the substrate.

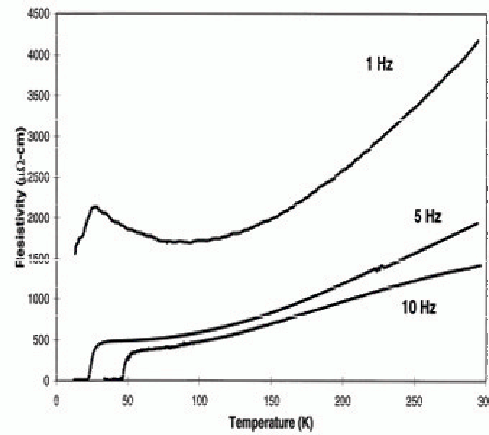


Figure 3.5: Effect of laser pulse repetition rates on quenched $YBa_2Cu_3O_{7-d}$ films [7]

3.1.9 Substrate Temperature

As mentioned before, MgO was chosen as a substrate because of its low dielectric losses, which makes it ideal for high frequency microwave applications. The temperature chosen was $724^\circ C$, as was optimized by van Staden [3]. A study was done by Kuriki [28] and various temperatures and parameters were analyzed in terms of T_c and J_c of a 30° grain boundary SQUID junction. It was established that a residual resistance ratio (RRR) of 3 would give high current densities of more than 5×10^6 A/cm² at 77 K. This was also proportionally related to the critical current J_c of the YBCO film, while T_c did not correlate well with J_c . Furthermore, it was established that the J_c peaked at $700^\circ C$, whereas T_c was consistently at between 89-90 K at temperatures above $700^\circ C$.

3.2 Problem Identification and Solutions

An overview of the standard PLD method and the critical parameters that will successfully produce a stoichiometric superconductive layer, has been given. A further improvement to the sintered target [29] and the recent discovery of YBCO (358), which has a higher T_c at about 102 K [34], could improve the reliability of devices operating in liquid nitrogen environments. Higher critical currents would be achievable. Further processing, such as the deposition of gold pads, is also easily done with different parameters in the same PLD system. With the ongoing research there are constant improvements, which will make the superconductive thin films more reliable in time.

The PLD chamber was built for single experiments. However, trying to optimize parameters becomes very time consuming. Most of the time taken in a deposition is needed for the pumping down of the main chamber to base pressure. A good base pressure ensures that most contaminant gas molecules, especially water vapour, have been extracted and that the initial deposition conditions are met.

Thus, the time needed to reach a base pressure of 2×10^{-5} mbar can be as long as four hours, and for a base pressure of 2×10^{-6} mbar up to 15 hours. This can be very time consuming when trying to characterize a new process where multiple parameter changes are required. In order to improve the existing system, a rotating six stage multiple substrate holder was designed that exposes only one substrate at a time, thus allowing six depositions to be done in succession with individual heating capabilities. An eight substrate heater was also build on a single rotating heater, see Appendix (Technical Diagrams).

To improve the surface roughness, two further modifications were built; based on the construction of DeLeon *et al* [20], a modification was done to enable Laser Assisted Molecular Beam Deposition (LAMBD) to be incorporated into the existing chamber. Later a further modification based on the Willmott *et al* [9] system was built to perform Pulsed Reactive Crossed Beam Laser Ablation (PRCLA).

3.2.1 Multiple Substrate Holder

The substrate holder incorporates a temperature sensor on each substrate holder and a heat source consisting of a cartridge heater that could be engaged and disengaged when rotating to the next substrate. Also, in between the substrate holders there is an intermediate position to allow for a pre-ablation to occur without contaminating the substrate. The other five substrates are covered by a special plate with an opening large enough to expose the substrate to the plume. There is also a water cooling system designed to cool up to the main substrate holder. There are two water channels that are drilled into the rotating shaft to the substrate holder, to allow for rapid heat transfer. Once the depositions are completed, the shaft would be turned back to the original position in the opposite direction.

3.2.2 Design Considerations

The target to substrate distance should be adjustable and changeable without breaking vacuum. This was accomplished by having an O-ring on the outside of the main shaft and fixing the centre to an outer external pipe. The shaft can now move linearly, while under vacuum, and is secured with a 6 mm cap screw to the outer rotating handle. The whole assembly was made of aluminium, except for the substrate heater assembly, which was made of stainless steel.

The modification helped speed up the experiments and resulted in several published articles [35], [36], [37]. There is, however, a 40°C degree heat loss between the cartridge heater and the substrate holder, which can be ignored when heating up to 500°C . The reason for the discrepancy is the surface oxidization taking place in the ambient oxygen environment. When heating to 724°C , the cartridge heater is at 764°C and has reached its peak energy density capacity, which in turn lowers the lifetime of the heater.

These modifications are shown in Fig. 3.6. It has been decided to replace the cartridge

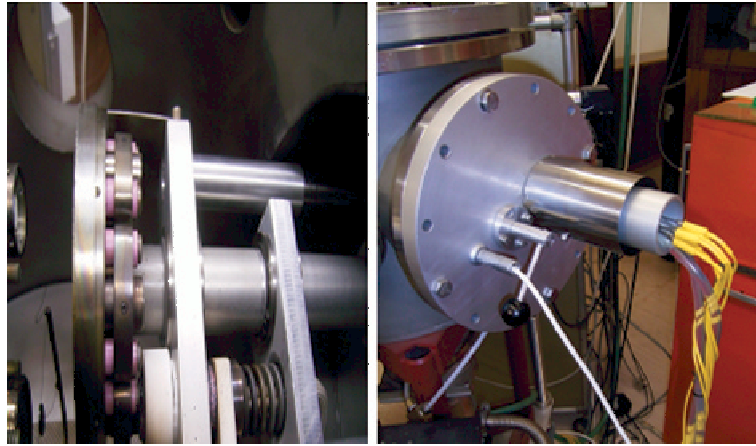


Figure 3.6: On the left is the rotating substrate holder with the cartridge heater. The right hand picture shows a release handle to position the heater and six temperature probes, with water cooling, to the substrate holder

heater because of the limited life span of about 40 hours. The new heater is based on a later design that was built for single substrate heaters. The conversion will entail replacing the cartridge heater with a radiant halogen light, which has the intensity to heat the substrate holder to 800°C without making physical contact.

3.2.3 PLD with Shadow Mask

The first attempt to improve the surface roughness, was to use the existing PLD system and create a particulate filter. A small 10 mm disc was used and positioned a third of the distance away from the target, as shown in Fig. 3.7. The idea was to prevent the large energetic clusters from depositing on the substrate. The disc was positioned, in direct line of sight, to cover the substrate totally. Only smaller atoms, ions and ionic species would be able to reach the substrate by following a curved path. The results showed improvement in the surface roughness. Unfortunately the deposition time increased threefold and thus an alternative method had to be found.

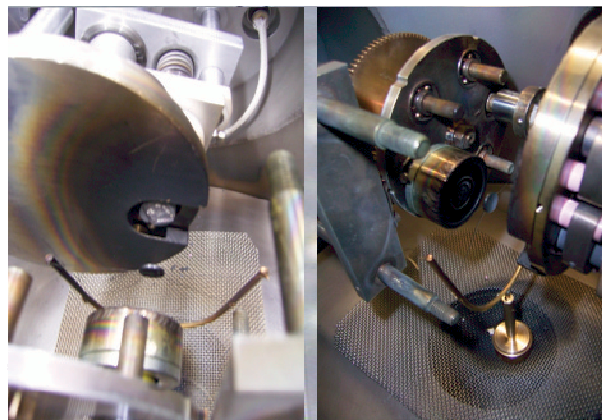


Figure 3.7: Rotating substrate holder with shadow mask

3.2.4 Laser Assisted Molecular Beam Deposition

The conversions done were based on research done by DeLeon *et al* [20] and Li *et al* [1]. This entailed separating the main deposition chamber into two chambers; the target chamber and the substrate chamber is shown in Fig. 3.8.

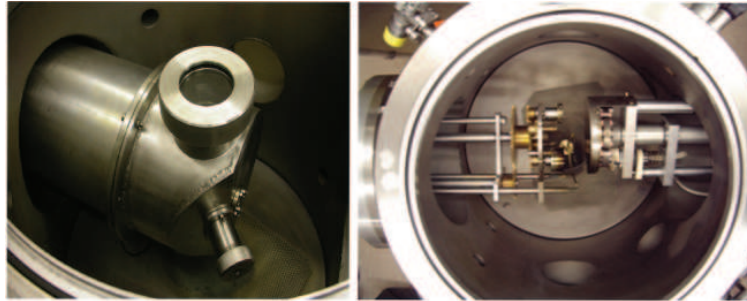


Figure 3.8: Conversion from standard PLD chamber (right) to laser assisted molecular beam deposition (left)

A pulsed valve on the outside of the chamber leads into the target chamber which, in turn, is separated by a supersonic jet from the substrate chamber, thus creating two different pressure chambers. The valve and laser are triggered by a pulse delay generator, so that the laser and the oxygen pressure are synchronized. There is a delay of $2.2 \mu\text{s}$ in the gas pulse reaching the target. This delay is caused by the mechanical action of the solenoid valve.

The pressure in the inner chamber can be set as high as a few atmospheres. A high concentration of oxygen or other gases is formed that reacts with the ablated species. They are then ejected at supersonic velocities into the evacuated chamber, via the jet, as is shown in Fig. 3.9. There are thus possibilities of creating new materials with higher concentrations of reactive gases in the future.

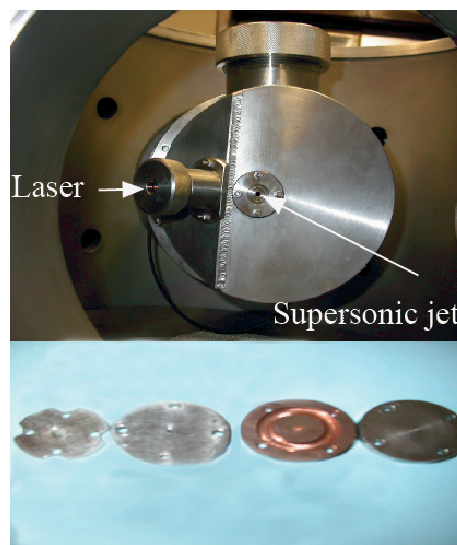


Figure 3.9: Laser is focused into ablation chamber and atoms, clusters and ions are accelerated into vacuum via a supersonic jet (interchangeable)

3.2.5 Pulsed Reactive Crossed Beam Laser Ablation

The standard PLD configuration is limited to a specific target-substrate distance to create good thin film uniformity. The plume is dependent on the reactive gas pressure and fluence. However, the surface roughness is in the region of 30 nm or more and bulk target material in the micrometer range is deposited onto the substrate as previously mentioned.

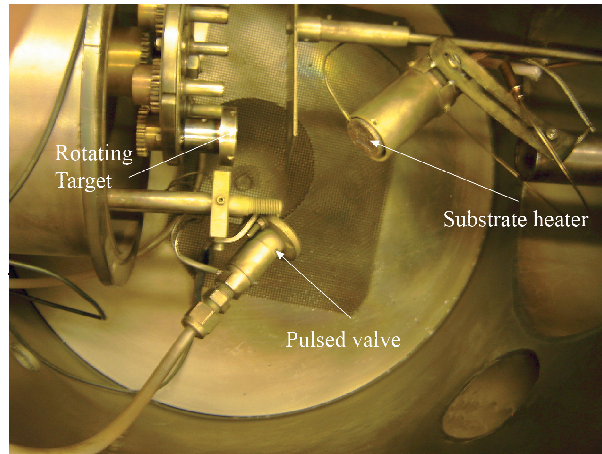


Figure 3.10: PRCLA with shadow mask

In the case of YBCO growth devices, the surface roughness should be in the region of 4 nm to 7 nm. An alternative method was investigated, whereby a shadow mask was positioned between the target and the substrate. The position of the shadow mask is important, as the substrate is totally shielded from any heavy particles in line of sight to the incident laser, as illustrated in Fig. 3.10. Thus, only lighter particles that are accelerated by the gas pressure valve will reach the substrate. The gas solenoid valve was positioned in the vacuum chamber. After the modifications were made the experiment was optimized by De Villiers [8] to improve the CeO thin film buffer layers, and successful YBCO JJs were achieved. The setup is shown in Fig. 3.11.

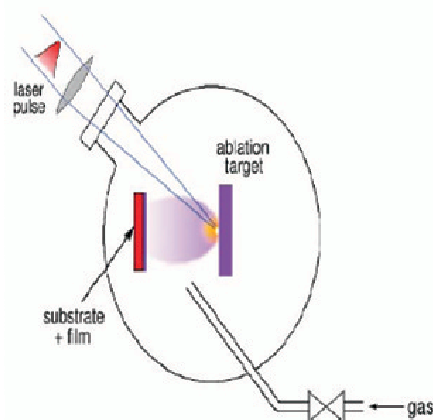


Figure 3.11: Schematic representation of pulsed reactive crossed beam ablation

In PRCLA the reactive gas valve trigger pulse is synchronized with the laser trigger pulse. The oxygen was pulsed into the vacuum, which means that highly reactive atoms collided and then accelerated from the target to the substrate under lower pressures than used in the PLD. This setup was based on the work done by A. Gupta and B.W. Hussey [38] in 1991, and subsequent research by Willmott *et al* [39].



Figure 3.12: Stanford Research Systems DG535 digital delay timer (top) connects to pulsed valve driver (bottom) used to synchronize the gas pressure valve and the laser pulse for PRCLD

Fig. 3.12 shows the pulse delay timer and the solenoid pulse generator used in the PRCLD.



Figure 3.13: (A) Photograph of laser plume when gas valve and laser are triggered simultaneously; (B) Photograph illustrates a 2.2 ms pulse delay between gas valve and laser [8]

Figure 3.13 clearly shows that the 2.2 ms delayed laser pulse luminescence becomes brighter. All parameters were kept the same, except that the laser delay was changed.

The graph in Fig. 3.14 depicts the time delay between the initial pulse that was sent to the gas solenoid valve. This valve, being a mechanical system, has two internal springs and thus has more delay than, for instance, a more expensive piezo electric valve. Interestingly, the change is very visual, indicating that there is a physical reaction between the oxygen and the ablated clusters. The delay was done in steps of 0.1 μ s until there was a significant spectral change. There are various parameters that

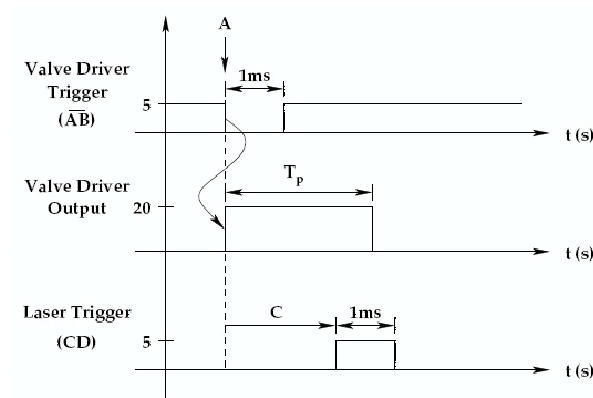


Figure 3.14: Delay pulses of the pulsed valve and the laser beam. [8]

influence the overall ambient pressure. For instance, the back valve pressure, pulse width and repetition rate all have an influence on the total ambient pressure.

By inserting a shadow mask the larger particulates of YBCO were filtered out and a droplet-free layer was produced. Fig. 3.15 shows the effectiveness of the shadow mask on the surface roughness [8].

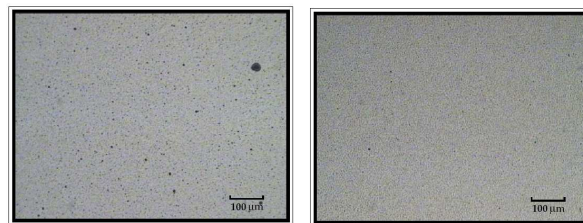


Figure 3.15: YBCO PRCLA without (left) and with shadow mask (right) deposition done by de Villiers [8]

3.3 Conclusion

Three modifications were done to the original PLD system. There was a fivefold improvement on the number of depositions done per run, achieved by modifying the substrate holder. Furthermore an additional LAMBDA facility was created and PRCLA with a shadow mask gave us the opportunity to deposit a droplet-free CeO buffer layer to the YBCO. The completed modifications have improved the current standard PLD system and have been cost effective. This also allowed de Villiers to create successful CeO bi-epitaxial YBCO Josephson Junctions [8].

The advantages of the PRCBLD was proved by Willmott *et al* [39] on work done on TiN. The degree of ionization of the plasma, in terms of the collisional process, is approximately two orders of magnitude higher than the standard PLD method. The total effective cross section of the atoms is four times higher than at ambient gas pressure. The rapid gas expansion allows atoms and ions to propagate at quasi

collision-free conditions, thereby avoiding collisional quenching and maintaining the reactivity as they strike the substrate. In general this method has distinct advantages over the standard PLD system.

P.R. Willmott's research group [9] created a droplet-free zone using the PLD system with two laser beams, as shown in Fig. 3.16. Here they suggest aiming two beams at two targets with diaphragm shields, which catch the droplets, allowing only fine ion species to strike the target. This option was not explored, due to chamber constraints, the reconstruction of the target holders, and the availability of only one excimer laser beam.

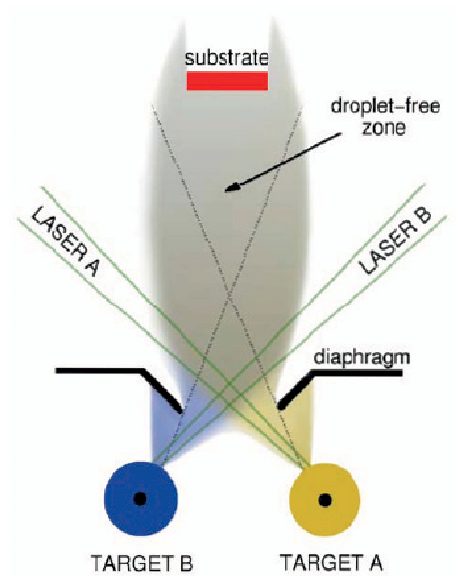


Figure 3.16: PLD droplet free zone described by Willmott *et al* [9]

After modifying the PLD system more users were able to do their research here, due to the time saved by having the six-substrate holder. It also gives researchers the opportunity to explore new materials, using the LAMBD system. Finally, with the PRCLD and shadow mask, it was possible to improve the surface roughness of CeO [8].

Chapter 4

Inverted Cylindrical Magnetron Sputtering

4.1 Motivation

Initially, pulsed laser deposition was the only facility available to our research group for YBCO deposition. On average a superconductor layer thickness is about 150 nm, and reproducibility of micro-structures becomes a challenge, especially when large particles are also frequently found on the substrate surface. Due to the surface roughness and microparticles which deposit on the substrate surface, an alternative method was investigated.

After the investigation, sputter deposition was chosen as the method most suitable for our process. After analysing both planar and off-axis sputter deposition, it was concluded that the off-axis deposition favored YBCO epitaxial growth [40]. This would enable us to sputter other complex materials. Other advantages are that the film shows a good adhesion, excellent film uniformity, and has bulk-like properties. The alternative, planar system is an on-axis method that causes re-sputtering of the deposited layer, which the off axis deposition does not do. Achieving a surface roughness of between 6 - 10 nm could now be possible, which would be better than that resulting from the existing PLD system used.

An inverted cylindrical magnetron sputtering (ICM) system is more cost effective than running an excimer laser, with a minimal amount of down time for maintenance. This chapter will focus on the design and construction of a simple DC Inverted Cylindrical Magnetron, and gives the results that were published [4], based on the thin films that were made with this system. The grown YBCO shows an overall surface roughness of 7 nm as opposed to films produced by the PLD system, that had a roughnesses of between 34 nm and 72 nm.

4.1.1 Basic Vacuum Considerations

The chamber design entails consideration of various stages of the sputter process. The base pressure achieved before the sputter process commences, the actual sputter pressure, and the pressure needed when the substrate is annealed, are the three main aspects to be considered. Since the base pressure is near 10^{-6} mbar and the working pressure at 10^{-2} mbar, there should be a bypass valve to isolate the turbo molecular pump from the deposition chamber during the actual sputter process. The use of a turbo molecular pump instead of a diffusion pump has definite advantages in terms of having potentially less carbon contamination arising from the heated oil.

4.1.2 Target Selection

The next consideration is to select the diameter and type of target, so that the deposition thickness is uniform over the entire substrate. Previous literature [40] shows that, specifically for YBCO, an off-axis type of sputter process is ideal for stoichiometric film growth. Fig. 4.1 shows the erosion of the target due to the highest density of the magnetic field.

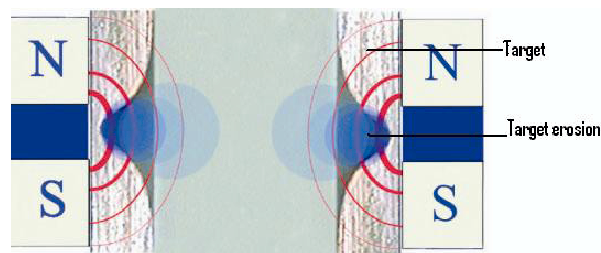


Figure 4.1: Cylindrical target displaying magnetic poles and ion confinement and target erosion.

A cylindrical target of diameter of 50.8 mm, height 25.4 mm and a thickness of 5 mm was chosen, as this diameter is a standard size, and would deposit a very uniform layer over a 10 mm x 10 mm substrate. There are various overseas target suppliers and targets of these dimensions are often stock items. The substrate size had previously been chosen by the research group, to be used as a standard size on all processes.

4.1.3 Magnet Design

Ideally, the magnets should be custom made of washer type magnets that have the north and south pole on either side. The magnets are positioned in the same direction on top of each other with a spacer in between them. These magnets are housed around the target and can be repositioned, so that the target erosion can be shifted up or down, in order to extend the target's lifetime.

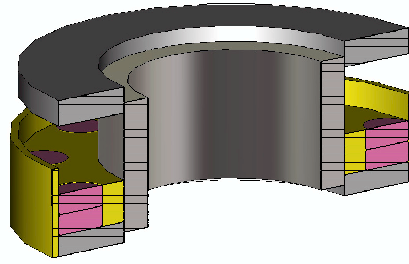


Figure 4.2: Rare earth button magnets are mounted between two mild steel rings in a copper cooling flange.

SmCo magnets were chosen for their high temperature tolerance of around 300°C before degradation. Copper was used as contact material between the target, magnets and water cooling. Standard button magnets were used, which were stacked between mild steel rings, as shown in Fig. 4.2. This method is very cost effective and flexible and allows for efficient cooling, as the button magnets fit into a copper flange. The copper flange also fits tightly against the target.

The whole assembly is surrounded by a copper cooling pipe that fits into the outer perimeter of the copper flange. The target, copper flange and SmCo button magnets are all on the same potential and are insulated from the outer housing. The whole system must also be vacuum tight.

4.1.4 Water Cooling

The water cooling method is dependent on power dissipation. The energy typically needed for the YBCO thin film layers was in the region of 400 mA at 180 - 200 V DC, which gives an average power of 72 - 80 W. The system has been successfully tested at a maximum of 500 W. The target, being the cathode, is electrically isolated from the outer anode body of the ICM which, in turn, is earthed.



Figure 4.3: The water cooling pipes are insulated from the outer housing and vacuum tight.

The target, magnets, copper cooling body and copper cooling pipe are also vacuum sealed. For safety purposes the cathode must be electrically shielded. A copper cooling pipe is used to cool the whole cathode assembly. A copper pipe is used in a closed loop construction to prevent water leaks, as seen in Fig. 4.3.

4.1.5 Material Selection

The material selection is often a compromise between the ideal choice and the machineability of these materials, considering magnetic fields, water cooling and vacuum conditions. Copper has a heat conduction of 401 W/mK, is non-magnetic and was chosen to cool the target and magnets. The copper sleeve fitted to the target should be tight to allow a good thermal heat conduction. The target is attached to a thin layer of copper, which in turn makes contact with the magnet holder. The temperature should be kept constant to prevent cracking. Bakelite was chosen as the insulator between the cathode and the anode. However, Teflon would have worked just as well. The anode could have been made of stainless steel or of aluminium. Aluminium has two advantages over stainless steel, namely better heat conductivity and ease of machining. The water cooling pipe was made of 8 mm copper pipe.

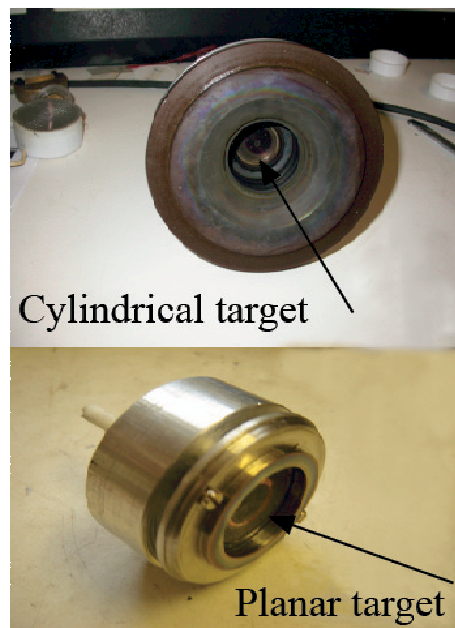


Figure 4.4: Insert conversion from from ICM to planar sputtering.

An insert was built to convert this ICM to a planar type of sputtering system, Fig. 4.4, using the same input power conditions. The added feature would allow for targets to be made inhouse by using a pellet press.

4.1.6 Dual Sputtering Magnet Design

A further sputtering system, with the potential to sputter two different materials, has also been constructed. This design was based on the first concept, using different materials and reconstructing the water cooling system (Fig. 4.5). The water cooling was changed to allow for up to 1.2 kW of cooling, to prevent the magnets and target from overheating.

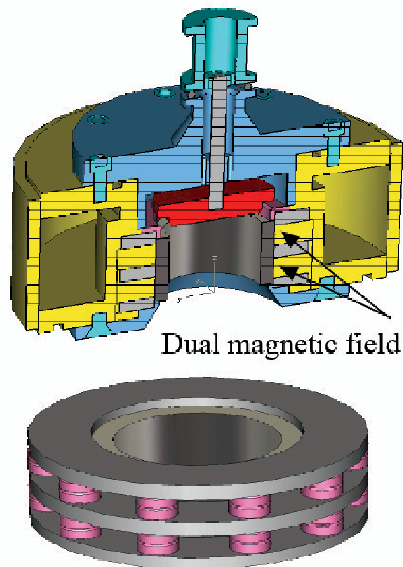


Figure 4.5: New dual sputtering magnet configuration with improved target cooling

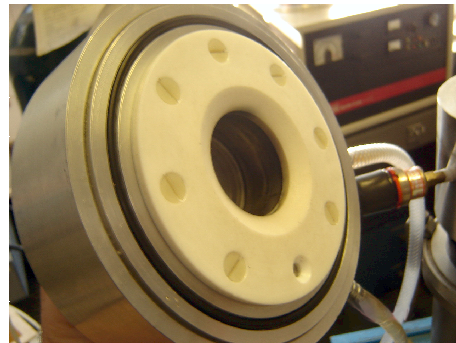


Figure 4.6: View of the completed dual sputtering head

The second sputter source was specifically designed for titanium sputtering at higher deposition rates. Fig. 4.6 shows the completed dual sputter target head assembly.

4.1.7 Substrate Heater

The substrate heater is one of the most crucial elements for the production of YBCO thin film layers. A responsive yet inexpensive system, that could heat up to 800°C in eight minutes, and also cool down in a short period of time, was required. Initially

experiments were done using copper coated with nickel. However, after heating in oxygen pressure and under vacuum, the protective nickel coating was not effective in protecting the copper from oxidization. The heater body was then made of stainless steel, which is less heat conductive, but shows a uniform heat dispersion over the surface.

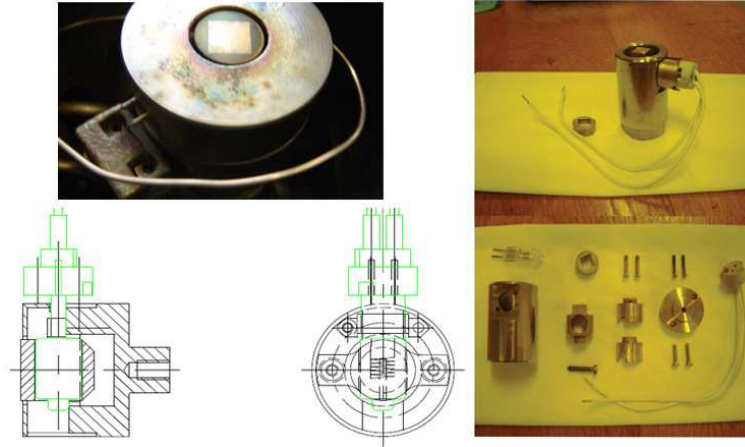


Figure 4.7: Two of four different substrate heater types that were built for various applications.

The power supply was specially designed to allow for slow, or soft, on and off response, so that the bulb's lifetime was lengthened and the temperature became more stable. The heat shield and heater housing were also made of stainless steel. A temperature probe is connected to the heater body, which has a removable heat shield. The substrate heater assembly is isolated from the outer housing and shield with ceramic washers. The outer body is positioned onto a water cooled pipe, via a rod and copper base, allowing the body to be kept at a temperature below 300°C .

The substrate heater body has been made of stainless steel, with a heat conductance of 16 W/mK , as opposed to copper at 401 W/mK . Due to the oxidative environment and high temperature of the YBCO growth conditions, the copper oxidizes and exfoliates.

4.2 Results of analysis of YBCO thin film and oxygen/argon reactive gas mix

These are results from analyses of different pressure ratios of Ar and O₂, which were done by van Staden [3].

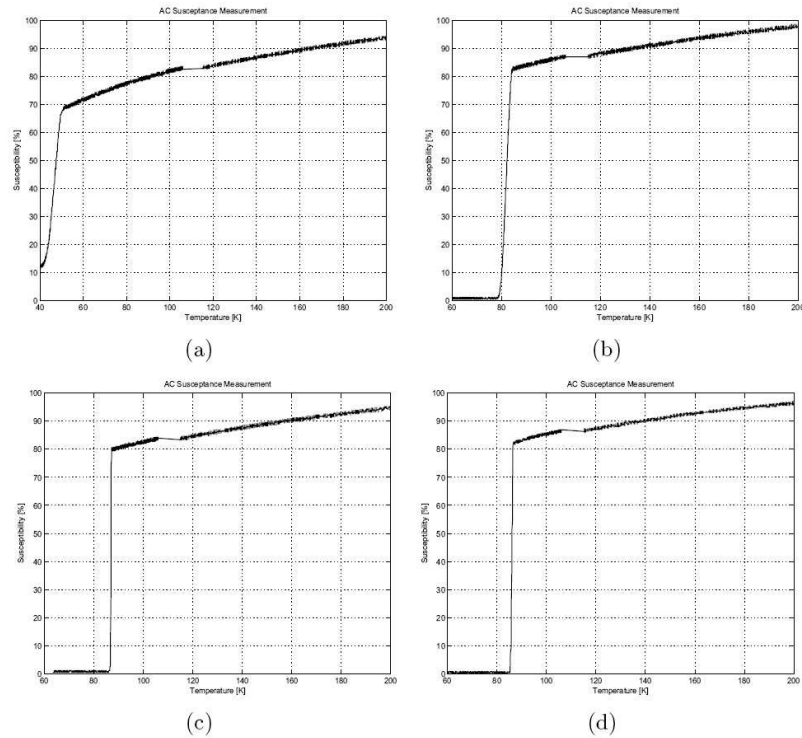


Figure 4.8: Susceptibility tests for oxygen/argon ratios of (a) 1:2 (b) 1:1 (c) 2:1 and (d) 4:1 at a constant total pressure of 150 mTorr [3]

The four graphs shown in Fig. 4.8 display the results achieved by using the newly constructed ICM [3] with reference to Table 4.1.

Table 4.1: Superconducting IV curves are shown with different oxygen to argon ratios obtained by ICM [3]

O ₂ :Ar Ratio	T _c [K]	ΔT [K]
1:2	43.5	10
1:1	82.8	5
2:1	87.2	0.6
4:1	86.7	1.2

From the data shown in Table 4.1, the optimal oxygen/argon ratio was found to be 2:1. The oxygen content, at twice the pressure of argon, has a T_c of 87.2 K and δT of 0.6 K.

4.3 Conclusions

The ICM was designed as an alternative deposition source to the expensive PLD system. It has been tested with a YBCO target, and has been successfully characterized by van Staden [3], Elkaseh [12] and de Villiers [8]. The surface roughness was about 4 nm, as opposed to the PLD surface roughness of 72nm (excluding particulates). This improvement would allow for multiple layered devices to be fabricated. The substrate heater was designed out of necessity as the previous one broke and the replacement would be 10 times more expensive than the new heater design. The heaters have been used extensively and, on average, the element lasts for 6 months. With a pulsed DC power supply the current ICM sputtering system will be able to sputter materials from non-conductive targets as well.

Even though the dual sputtering head was based on the previous ICM design, which has good plasma ignition and sustainability, this configuration is currently unstable with a DC voltage supply. Further work will have to be done to see if the RF simulations, that were done at 13.56 MHz will be stable. A Pulsed DC supply has been developed specifically for the ICM and is close to completion. This work is still in progress.

Chapter 5

Argon Ion Mill

5.1 Introduction To Argon Ion Milling

Argon milling is an etch process referred to as dry etching, as opposed to wet etching where a liquid is used for etching specific materials. In wet etching fine or small resolution structures are often over etched, since etching occurs under the photo resist. Argon ion milling, on the other hand, is a more controlled system, which has become the preferred method in etching nano structures, especially in the construction of Josephson junctions in superconductors, where the physical dimensions are critical. In this method positive ions are created from a gas, such as argon, and accelerated toward a patterned surface so that the surface would be exposed to ion irradiation, and atoms would be sputtered off.

Dry etching has become a common method used in micro- and nano-fabrication. It can be used on thin film layers and, being anisotropic, does not require special considerations specific to the material to be etched, as is the case with wet etching processes. An RF magnetron plasma source is used in dry plasma processing at low pressures, $1.3 - 3 \times 10^{-4}$ mBar, in an external magnetic field. The magnetic confinement contributes to the maintenance of the plasma by reducing the electron losses to the outer chamber walls. The RF power supply has a frequency of 13.56 MHz and a waveform of $V_{rf} = V_o \sin(\omega t)$. This method is controllable in terms of the plasma energy and acceleration voltage, with excellent resolution capabilities.

5.1.1 Basic Design

The initial design was based on a multi cusp source as used by Rottier [26], which consisted of a multi cusp RF system with a water cooled antenna. The system had a single extraction hole which did not have a uniform etching profile. Also, the sixteen magnets used for containing the plasma were water cooled and exposed to corrosion. The antenna is water cooled and made from 6 mm copper pipe that is sealed by two teflon fittings with O-rings against the top flange.

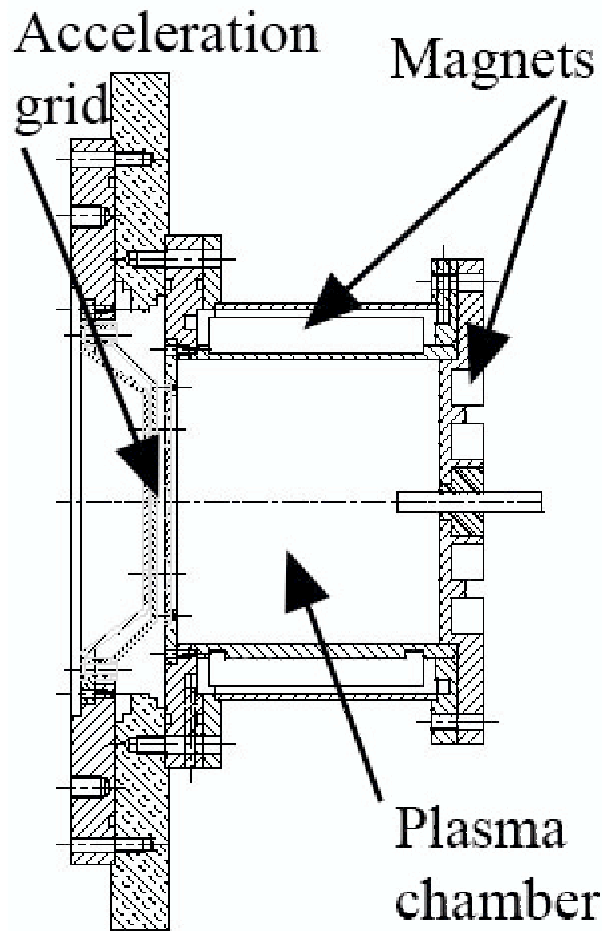


Figure 5.1: Diagram of the argon ion mill showing the chamber confining magnets surrounding the plasma chamber and the acceleration grids

The plasma chamber comprises a cylindrical chamber of stainless steel with 16 SmCo magnets containing the plasma and four SmCo magnets attached to the lid, as shown in Fig. 5.1.

5.1.2 Modifications On The Plasma Extraction

The main modifications done after the initial construction of the argon ion mill was the removal of two single hole acceleration plates. Although the ion beam diverged to 20 mm, a centre region of 10 mm would etch at a higher rate and create a very non uniform etch profile over a diameter of 20 mm. By removing two single holed acceleration plates and replacing them with three aligned multi-holed grids as an acceleration system, the beam profile was changed. The grids were placed above each other and were aligned with 2 mm teflon spacers. The distance was chosen after considering the maximum acceleration voltage needed between these plates.

A 2000 V spacing was calculated using Paschen's law. Paschen defines the relationship

between gas pressure and breakdown voltage as

$$V = \frac{a(pd)}{\ln(pd) + b} \quad (5.1.1)$$

where V is the breakdown voltage, p the pressure, d the gap distance in meters, and a and b gas constants.

The gas constants a and b in atmospheric gas of 760 Torr are given by $a = 43.6 \times 10^6$ V/atm-m and $b = 12.8$. Taking the breakdown voltage as a function of pressure and gap distance (pd), the formula can be differentiated in terms of pd and equated to zero, to give the lowest voltage.

The lowest voltage is given when $pd = e^{1-b}$

From Paschen's law it is evident that the breakdown voltage depends on the distance and pressure between two parallel conductive surfaces.

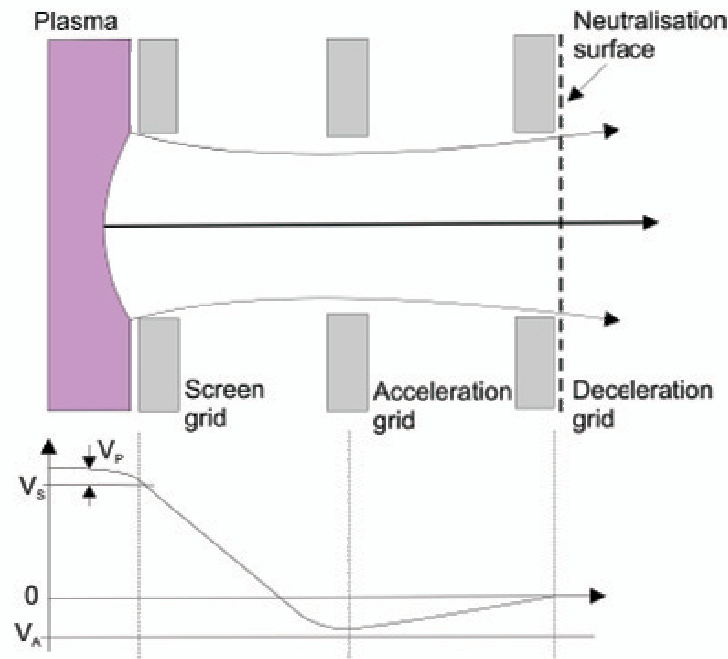


Figure 5.2: Voltage potential across three grid ion extraction plates [3]

The distance was estimated taking Paschen's law into consideration at a working pressure of 4×10^{-4} mbar. A distance of 2 mm was selected between plates. The grids were perforated stainless steel and the holes were 0.5 mm in an array of 1.5 mm centre-to-centre spacing. The approximate area of the grid-hole-array was circular, with a diameter of 40 mm. The screen and deceleration grids were widened to 0.8 mm and the acceleration grid was kept at 0.5 mm to allow for ion extraction, as depicted in Fig. 5.2.

5.1.3 Vacuum Considerations

As opposed to DC sputter deposition, the argon ion mill's working pressure is in the region of $1.3 - 2 \times 10^{-4}$ mbar. It is thus important to achieve a good base pressure before the working pressure is set. The difference in these pressures depends on, the amount of argon added, which constitutes the plasma. Once the argon ions have been generated they are accelerated by a three grid system. The pressure is inversely proportional to the etch rate of the ions. The lower the pressure, the higher the etch rate up to a point where the argon plasma is reduced, due to fewer ions being available.

5.1.4 Magnetic Plasma Containment

The plasma is generated by applying a 50 Watt 13.56 MHz RF signal via a variable impedance matching circuit to a water cooled antenna. The antenna is electrically isolated from the stainless steel vacuum chamber. The plasma is then created by matching the resonance frequency to that of the frequency at which argon gas is ionized. When operating the plasma at low pressures, in the order of $1.3 - 3 \times 10^{-4}$ mbar, the ions and electrons produced would be rapidly lost to the outer chamber walls by the lack of binary collisions by either the ions or electrons and the neutral gas molecules of the argon feed. Once the plasma has been ignited, it must be contained magnetically to prevent any thermal heat transfer to the inner walls of the chamber. This is done by positioning sixteen SmCo magnets in a multi cusp formation with alternating North and South polarity. The lid contains another four magnets to further confine the plasma.

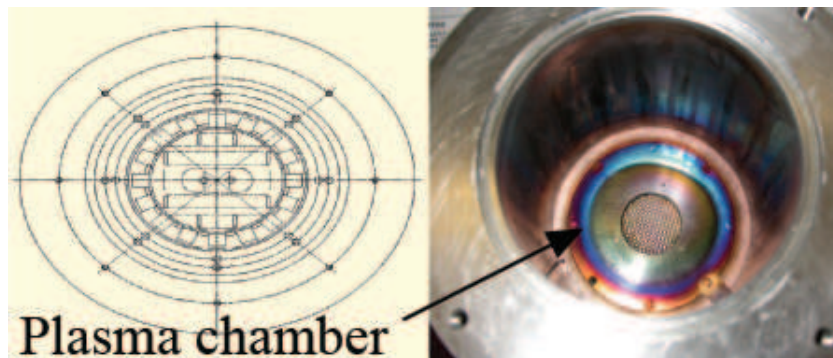


Figure 5.3: Plasma confinement diagram (left) and inside view (right) of actual plasma chamber with new acceleration grid

Fig. 5.3 shows a diagram of the 16 confining magnets and an internal view of the plasma chamber with the top acceleration grid. With this arrangement there is a magnetic field free region in the middle of the plasma chamber, which creates a more homogeneous plasma. This configuration is effective in confining the electrons inside the reactor when the mean free path of fast electrons is equal to or larger than the reactor's chamber size. A positive voltage is applied to this chamber to aid in the extraction process.

The ion current density J_i can also be calculated as

$$J_i = \sigma_i n_0 e \sqrt{\frac{kT_e}{m_i}} \quad (5.1.2)$$

where J_i is the ion current density, σ_i is the ionization cross section, n_0 is the neutral gas density, k is the Boltzmann constant, T_e is the plasma electron temperature and m_i is the ion mass.

5.1.5 High Voltage Requirements

The high voltage needed for the process is in the range of ± 3000 V, depending on the ion current needed. In the case of YBCO etching of fine structures the ion current should be kept at 500 V positive and 500 - 1000 V negative to prevent any ion damage to the thin film. The secondary currents on both high voltage supplies are also monitored and will give a good indication of whether the cooling water needs to be replaced.

In plasma etching, high energy ions with a mass of M_p and a velocity distribution $g_p(v, r, t)$ will have a density $n_p(r, t)$ and radicals or chemically active molecules, respective of mass M_r , velocity distribution $g_r(v, r, t)$ and a density of $n_r(r, t)$ and both will strike the substrate surface, it is then possible to calculate the flux of the materials ejected from the surface by dry etching as [41],

$$\begin{aligned} N_s V_s |_{r_0} = & n_p(r_0) \int Y_{etch}^p(\epsilon_p) \left(\frac{2\epsilon_p}{M_p}\right)^{1/2} g_p(v, r_0, t) dv \\ & + n_r(r_0) \int Y_{etch}^c(\epsilon_p) \left(\frac{2\epsilon_r}{M_r}\right)^{1/2} g_r(v, r_0, t) dv \end{aligned} \quad (5.1.3)$$

where $Y_{etch}^p(\epsilon_p)$ and $Y_{etch}^c(\epsilon_p)$ are the etching yields of ions (p) and of radicals (r) and N_s and V_s are the number density and velocity of the molecules ejected from the substrate material. The formula (5.1.3) shows the contributions of the physical and chemical etching, respectively.

The velocity distribution functions can be normalized as

$$\begin{aligned} \int g_p(v, r, t) dv &= 1 \\ \int g_r(v, r, t) dv &= 1 \end{aligned} \quad (5.1.4)$$

The etch rate can thus be calculated with respect to the atomic density ρ

$$\begin{aligned}
R_{etch} = & \frac{n_p(r_0)}{\rho} \int Y_{etch}^p(\epsilon_p) \left(\frac{2\epsilon_p}{M_p}\right)^{1/2} g_p(\nu, r_0, t) d\nu \\
& + \frac{n_r(r_0)}{\rho} \int Y_{etch}^c(\epsilon_p) \left(\frac{2\epsilon_r}{M_r}\right)^{1/2} g_r(\nu, r_0, t) d\nu
\end{aligned} \tag{5.1.5}$$

Thus $g_p(\nu, r, t)$ has a high anisotropic distribution and is beam like, while $g_r(\nu, r, t)$ is an isotropic thermal distribution in front of the substrate or electrode.

Chemical or wet etching presents an alternative method to create thin film structures. The main drawback is the resolution of this method, since the chemical reaction etches in two directions. The possibility of undercutting the structures below the photoresist limits use of this method to above sub micron structures.

5.1.6 Water Cooling

A water cooling jacket is situated on the outside of the plasma chamber, between the magnets and the outer enclosure. The lid has a water pipe around the SmCo magnets which then leads to the substrate holder that is also cooled. Since the plasma chamber is at a positive potential, the water used must be distilled and the conductivity must be monitored regularly. Once the conductivity becomes too high, the leakage current changes and the maximum voltage of 3000 V cannot be reached.

5.1.7 RF Antenna Matching

Between the RF power supply and the ion mill matching circuit, an isolation transformer separates the high voltage of the mill head from the power source. Two variable capacitors allow for coarse and fine adjustments to adjust the resonance frequency. Fig. 5.4 shows a schematic and a circuit diagram of the RF matching circuitry.

5.1.8 Substrate Holder

The substrate holder was designed to hold a 10 mm × 10 mm × 0.5 mm substrate. It has the possibility to rotate in two planes to the incident ion beam. The angles for step edges were determined by van Staden [3]. This substrate holder fits onto a water cooled stand, allowing the substrate to be cooled while milling takes place.

Fig. 5.5 shows the versatile water cooled substrate holder.

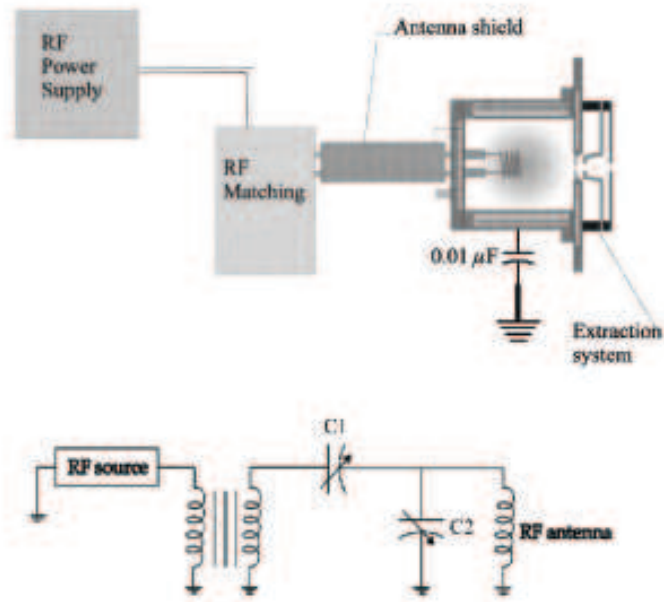


Figure 5.4: Multi cusp schematic with RF matching circuit [3] [10].

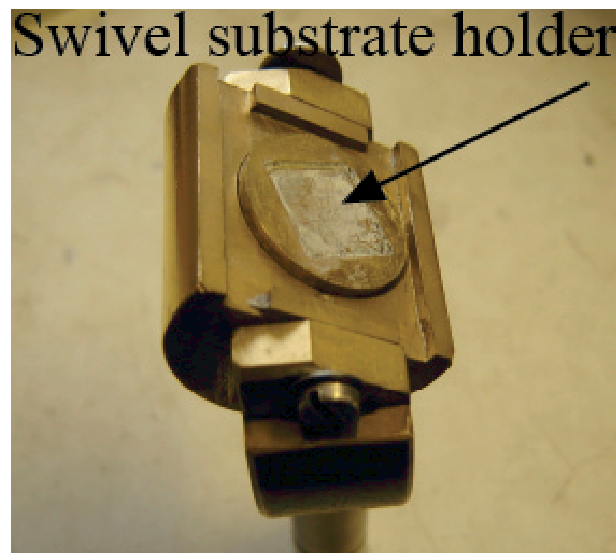


Figure 5.5: Fully adjustable substrate holder used to mill step etch profiles

5.1.9 RF Shielding

An important safety consideration is the RF radiation that is emitted during the ion milling process.



Figure 5.6: RF shield designed around the argon ion mill

A sheet metal box was constructed around the mill and measurements were made. With the shield in place,(Fig. 5.6), the radiation was measured and found to be within the safety specifications.

5.2 Conclusion

Originally, the system was built with a single 2 mm extraction hole and two electrostatic acceleration lenses. After realizing that the beam was not uniform, a system embodying a new concept was built. This three gridded design was successful and has been used extensively by the superconductor group. A possible improvement would be to build a magnetic filter which was implemented by Ji *et al* [42]. This addition should be investigated and the system possibly incorporated, into the existing chamber.

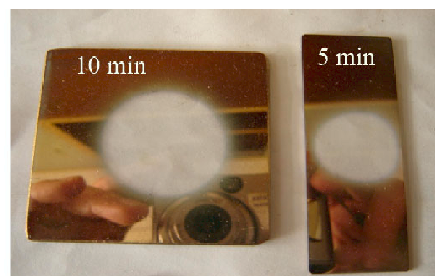


Figure 5.7: Gold plated glass slide showing a 10 min (30 mm diameter) and 5 min (22 mm diameter) ion beam etched area

The plume is uniform over the area of a 22 mm diameter circle and has a total area diameter of 30 mm. This has been proven experimentally by coating a glass slide with 50 nm of gold and milling it at different times, seen in Fig. 5.7.

Chapter 6

Lithography

6.1 Introduction

A need for more cost effective methods of large scale lithography for the purpose of manufacturing integrated electronic circuits is being industry driven towards the nanometer scale. Optical UV lithography was briefly discussed in the device fabrication process. These methods are limited to their wavelengths, and so alternative methods such as e-beam, AFM, STM, FIB, near field electro spinning, nano imprint lithography, AFM dip pen and supra molecular nano stamping are currently being used. In this chapter a few of these methods have been investigated.

Modifications were done to a standard Nanosurf AFM system enabling the user to do lithography over a larger area. Furthermore, a new concept was developed to produce constriction and tunneling junctions, using a 266 nm Neodymium Yag laser to create YBCO Josephson junctions. A further adapter was built to hold a linear stepper motor in the z plane. The AFM was removed with only x-y-z linear stepper motor actuators in place. This allowed fine control in all three dimensions (x,y,z), thus creating the possibility of using a laser fibre optic system as a lithography tool [43].

6.1.1 E-Beam Lithography

E-beam lithography has the capability of reaching structures with a resolution of less than 20 nm in a mask-less process. The industrial e-beam writing systems are very expensive, and so modifications were made to SEMs, such as beam blanking and additional software for locating the position of the lithography process. E-beam lithography is a tedious and time consuming process. It is thus necessary to work in two stages. An optical lithography process is first completed for structures up to micrometer resolution. Special alignment points are incorporated into the first lithography process, to ensure that reference points for the second e-beam lithography stage are in place. The substrate is re-coated with an e-beam resist and the SEM scans the surface at high raster speeds, so that no developing of the photoresist occurs. This photo resist

is UV insensitive and electron energy dependent. The e-beam lithography pattern is then aligned and the writing process can commence. The electron energy dosage is dependent on the specific e-beam resist.

The following formula applies

$$\begin{aligned} \text{Dose} \times \text{exposed area} &= \text{beam current} \times \text{exposure time} & (6.1.1) \\ &= \text{total charge of the incident electrons.} \end{aligned}$$

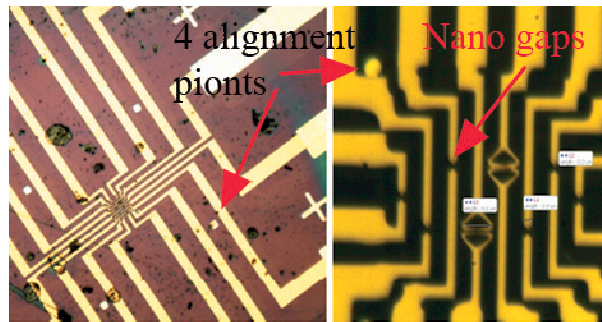


Figure 6.1: Combination of optical and E-beam lithography with four alignment points as was done at University of Pennsylvania [11]

Converting existing SEMs made this method accessible to many research groups worldwide. Unfortunately, there are some drawbacks, such as the long exposure times, beam drift, beam instability and high vacuum conditions, which limit the materials used to those that do not degas.

Fig. 6.1 shows nanostructures that were processed at the University of Pennsylvania. A three stage process was used incorporating various lithography methods to ultimately produce a 2 nm gap. The process started by using UV photolithography for large structures, followed by an e-beam lithography process, to reach a resolution of 30 nm. Thereafter a controlled current was applied, causing electron migration to occur, where nanometer gaps were achieved.

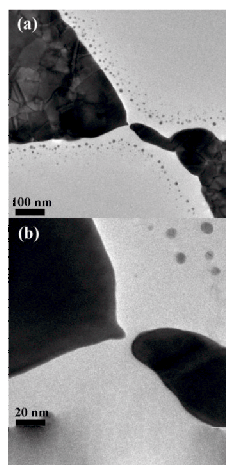


Figure 6.2: A 2 nm gap done by e-beam lithography and electron migration [11]

Fig. 6.2 shows a TEM picture of the previous e-beam lithography process shown in Fig. 6.1, done by Johnson *et al* [11].

6.1.2 AFM Lithography

An atomic force microscope (AFM) is a useful microscope with added features that enables lithography processes to be done. There are options of applying positive and negative voltages to the cantilever, or applying certain pressures to the cantilever. This enables oxidative or nanoploughing processes to be done. Our Nanosurf AFM system has a limited scanning range of $52\ \mu\text{m}$ with a fixed sample holder. Once the image is being scanned the sample holder cannot be moved. All the positioning is done manually by using the internal camera to view the position. The fixed sample holder was replaced by two x-y linear stepper motor controllers, and with some team effort, the software interface also became operational.

6.1.3 Modification of AFM

The first modification done to the AFM was an x-y stage that was built to fit onto our existing Nanosurf AFM stand.

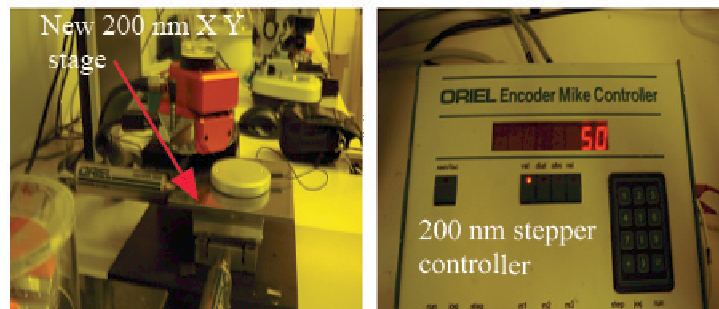


Figure 6.3: Multistage control box to control the x-y stage of the AFM.

A resolution of 200 nm steps is made possible with this new stage. The movement can either be stepped, jogged or run continuously, (Fig. 6.3). The advantage is that, while scanning an image, the stage position can be stepped to an exact location. This is imperative when a lithography process such as nano-scratching or oxidization of a surface at a specific position is done. This system has a resolution of 200 nm over a total area of $5\ \text{mm} \times 5\ \text{mm}$. The AFM has a resolution of 1.1 nm in the x-y plane. The controller also has the ability to connect via an RS232 serial port to a computer and run automatically off a program.

AFM nano-scratching was demonstrated by Elkaseh [12], (Fig. 6.4). He has also been able to show a tunneling type of junction by eroding a furrow over the entire length of the YBCO microstrip, keeping a residual thickness to allow electron tunneling to occur.

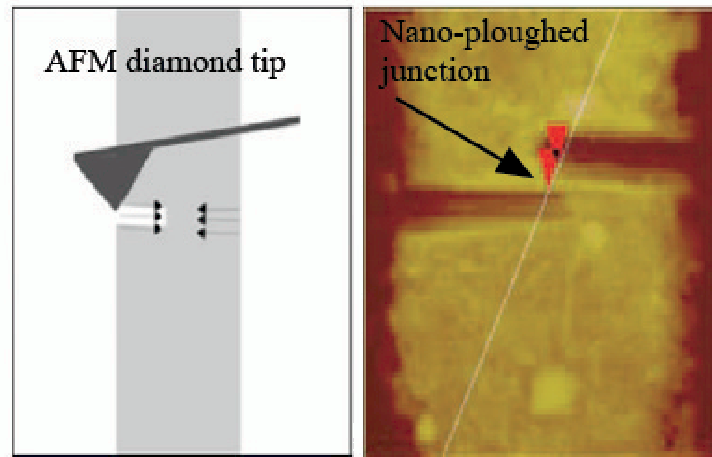


Figure 6.4: The picture on the left shows the AFM scratch process, and on the right the actual YBCO constriction junction is shown [12].

6.1.4 Laser Assisted Beam Lithography

The method entails using standard optical lithography and completing 10 YBCO microstrip lines varying from 4 to 8 μm . Once a microstrip has been made, a pulsed Nd-Yag laser 213 nm is used to modify existing dimensions and create nano-constrictive junctions.

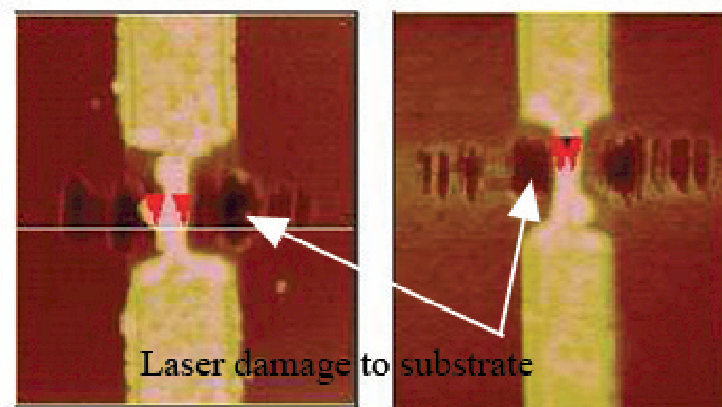


Figure 6.5: AFM laser-etched constriction junction at 1,64 μm and a sub-micron constriction junction at 703 nm [4]

The aim has been to prove that, by precise positioning and ablating microstrips, it was possible to create constriction and tunneling Josephson junctions, (Fig. 6.5). It was also shown that constrictions in the nanometer range were made [4]. The possibility of using the AFM to further scratch or modify this junction with the new x-y stage should now be possible.

6.1.5 Future Direct AFM Writing

After some modern systems had been analysed, the AFM (1.1 nm resolution) proved to be the easiest and most cost effective method by which to create a nano-lithography tool. Carbon nano tubes have been synthesized onto AFM tips by Bouchiat [13], (Fig. 6.6).

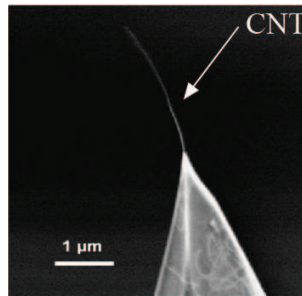


Figure 6.6: Self assembled growth of CNT-tip on conventional imaging AFM tip [13]

The idea is based on the high electric field strength AFM oxidization method. Here, moisture levels are controlled and a voltage of approximately 10V is applied to an AFM tip. This in turn induces a high electric field between the metallic surface and the AFM tip, causing oxidization to occur.

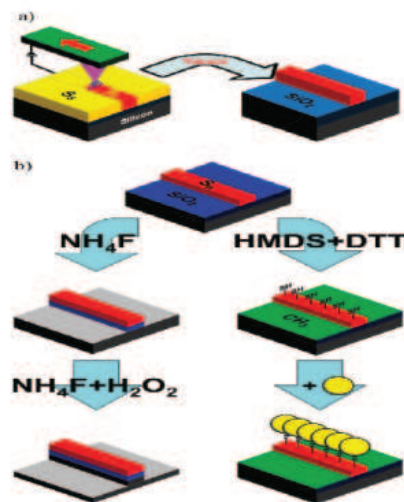


Figure 6.7: AFM sulphur photolithography done by Germain *et al* [14]

A similar idea is application of a positive 12 V bias to the substrate to induce a high field exceeding 10^9 Vm^{-1} across the conductive AFM tip. In this method a sulphur base resist is used. By applying a high electric field directly to a surface, the sulphur resist molecular structure changes to S_8 and becomes insoluble in toluene, similar to a negative photoresist. A silicon surface was coated with sulphur and the high field caused polymerization of the sulphur [14]. Patterns of 25 nm in width can be formed at high speeds of up to $200 \mu\text{m}$ per second. The layer is then chemically developed and as the sulphur track is etch resistant, the sulphur can be submersed

into hexamethyldisilazane and dithioerythritol, so that gold nanoparticles can self-assemble onto the functionalized sulphur tracks, (Fig 6.7).

6.2 Conclusion

It is now possible to do nano-scratching or oxidative lithography over a larger area. The working area was enlarged from $50 \times 50 \mu\text{m}$ to $5 \times 5 \text{ mm}$ in steps of 200 nm. A new concept of using a focused laser beam to create constriction and tunneling junctions was also devised.

Another option to improve the lithography system is to use an optical fibre laser system for direct laser writing. This could be used for larger dimensions in the micrometer range. The aim is to develop a cost effective simple nano-lithography system that can be used for prototyping new concepts, without the delay of having to wait for weeks for a mask to be fabricated. Most of the hardware and software is in place and finding the optimal solutions is going to be a new challenge.

Chapter 7

Testing Facility Modifications

7.1 Introduction

The Superconductor And Nano Device (SAND) research group consists of three sections, who research low temperature niobium at 4 K , high temperature YBCO at 92 K and a third group that focuses on nano-devices, such as solar cells, pressure sensors, micro silver switches and gas sensors. The most important part of manufacturing a device is the ability to test the quality of the thin film and the device non-destructively.

For low temperature (niobium technology) cryogenic testing, a two-stage CryoMech ST405 pulse tube refrigerator is able to cool to a temperature of 2.6 K, for rapid single flux quantum (RSFQ) circuit testing. There is, however, noise interference, which makes it impossible to measure small signals in the millivolt range and the Josephson junctions in the circuit are prone to magnetic flux trapping.

One aspect that must be taken into account, is how to shield the low temperature circuits as the cooling progresses. Magnetic fields, induced by the noise of the main compressor of the cryogenic cooler, vacuum pumps, as well as the effect of the earth's magnetic field, must be kept to a minimum. Modifications were made on both the low and high temperature cryogenic coolers to allow testing and characterization of circuits and thin films.

7.1.1 Thin Film Chip Mounting

The materials used to mount the chip must be non-magnetic and the PCB should have only copper tracks to prevent any flux trapping. The chip housing is made of niobium, which changes to a superconductive state at about 9 K, and thus becomes a magnetic shield due to the Meissner effect.

The PCB with all the connections positioned around the chip opening is mounted on the niobium base with three 1.4 mm brass screws (Fig. 7.1). The IC is attached to the

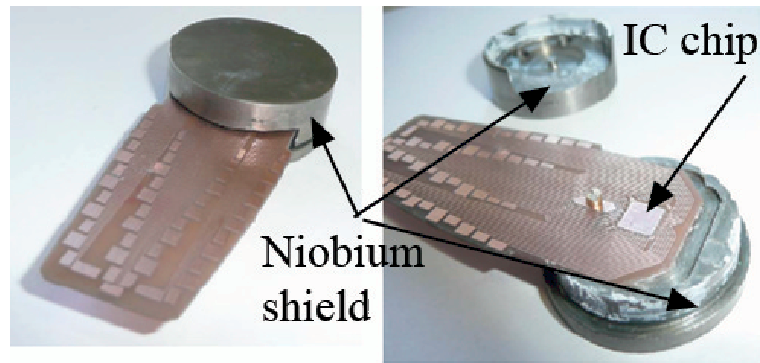


Figure 7.1: Niobium superconductor chip holder with wire bonded IC constructed to shield the RSFQ circuit from external magnetic fields

niobium shield with heat-sink paste (Dow Corning). Different heat-sink pastes were first tested by measuring the temperature of the surface of the chip. This was done by measuring the resistance of a niobium track, which has a direct relation to temperature measured. Discrepancies of up to 40 K were found between various heat-sink pastes. The chip is then wire bonded directly to the copper tracks of the PCB. The niobium lid and base create a magnetic field shield surrounding the RSFQ circuits on the chip. The opening slot is kept close to the PCB to minimize magnetic field penetration. The chip housing is attached to the second stage of the cryogenic cooler.

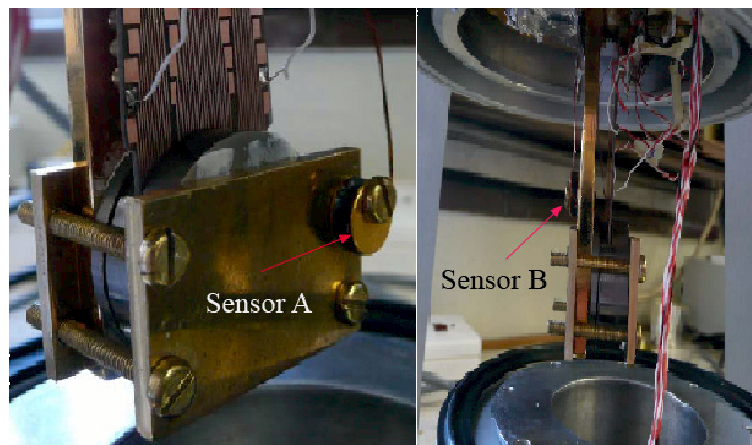


Figure 7.2: Niobium superconductor RSFQ chip holder, attached to the 2.8 K cooling stage, with two temperature sensors A and B

There are four brass bolts and two brass plates securing the chip assembly to the second stage of the cryogenic cooler. Two temperature probes are positioned independently to monitor the chip holder and the second cooling stage as a comparative measure (Fig. 7.2).

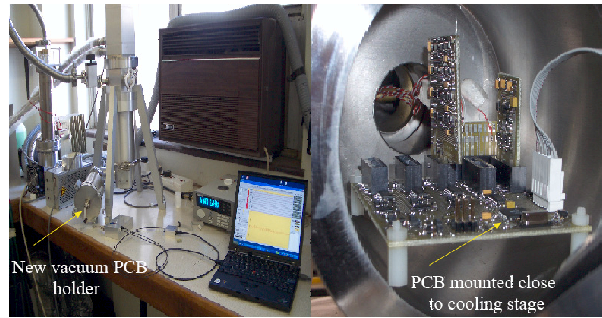


Figure 7.3: New vacuum chamber mounted close to second stage cooling for minimum heat loss and improved noise reduction

A special vacuum chamber was built for an electronic circuit, close to the cooling stage to minimize the thermal losses through the cables, and also to shield the circuitry from electrical interference (Fig. 7.3).

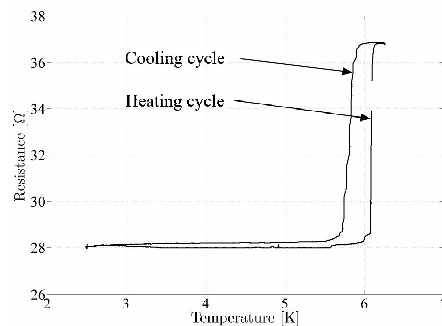


Figure 7.4: Resistance plot indicating the superconductive transition, which only occurs with the shield on.

To allow niobium films to become superconducting the static or dynamic magnetic fields had to be shielded. Tests were done on a niobium strip line and a resistance to temperature graph was plotted with the niobium shield on and off. It was established, that without the superconductive shield, the critical magnetic field strength was exceeded and the niobium strip did not become superconductive. Fig. 7.4 shows the cooling and heating cycle of the niobium superconductor strip, with the shield on.



Figure 7.5: Measurements of an RSFQ test circuit with the compressor system switch off (left) and on (right)

In the cryogenic COSL/RSFQ test systems thermal noise has been eliminated, but magnetic shielding still needs to be improved. Low-frequency inputs can be reliably supplied to the device under test, and sub-millivolt outputs measured. Fig. 7.5 shows a signal applied with the niobium shield in place. It can be seen that the noise levels of the cryo-refrigerator system still pose a major problem. As soon as the cooling system is switched off the signal can be clearly measured.

7.1.2 Susceptibility and Four Point Probe

An attempt was made to integrate both the susceptibility and resistivity tests simultaneously on a YBCO superconductor thin film. The probe head was made of copper and teflon, and made to fit a 10 mm x 10 mm x 0.5 mm substrate. The two pancake coils are on either side of the thin film substrate, surrounded by teflon to prevent electrical short circuits, making up the susceptibility test. Four spring loaded contact pads were positioned at the corners of the substrate, as shown in Fig. 7.6, and both types of measurement could be done.

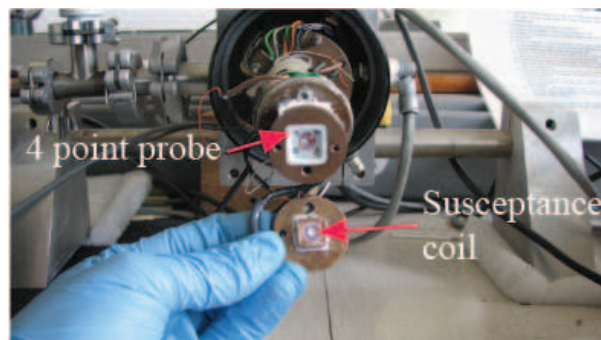


Figure 7.6: High temperature cryogenic cooler with susceptibility and four point probe resistance measurement capability

7.2 Conclusion

In this chapter various modifications were done to both high and low temperature testing facilities. For the HTS cryogenic test facility a combination of a resistive and susceptibility test system was built with special phosphor bronze spring loaded contacts. Unfortunately it was found that the HTS layers that were tested were all in the region of 150 nm to 200 nm thick, and exposed to vibrations on this system. These vibrations caused the pressure contacts to puncture the layer and create structural damage. For thicker layers above 500 nm this problem should not arise. New contact springs will have to be sourced to overcome this damage. Experimental results showed that the niobium shield was successful in limiting the electro-magnetic interference fields. However, the noise generated by the cryogenic cooling system, could not be sufficiently shielded. A possible solution would be to replace the stepper motor on the head of the cryogenic cooler with a DC motor.

Chapter 8

Overview of Results

The goal of this thesis was to show that it was possible to upgrade various processes that were needed to create thin film devices at a minimal expense. Five areas were targeted and various modifications were done, as well as designing and constructing an inverted cylindrical magnetron sputtering system with a new type of substrate heater, that proved to work well in various systems [3].

Modifications done to the PLD system included pulsed reactive laser deposition, laser assisted molecular beam deposition and a multiple substrate holder. Eight co-authored articles have been written by researchers using these modifications. Numerous students of iThemba Labs [44], the University of the Free State [45], the African Laser Centre, University of Lesotho, The Centre of Energy Research and Development at the Obafemi Awolowo University in Nigeria [35], [36], [37], [46] and students at the University of Stellenbosch [12], [47] have successfully used the systems.

The design and construction of the DC inverted cylindrical magnetron led to a further co-authored article [48] and one as first author [4]; the substrate heater was also used in both PLD and ICM systems.

The construction, commissioning and modifications of the argon ion mill proved to be crucial in replicating fine structures for device fabrication. One possible additional modification would be to mount a Peltier cooler to the substrate holder to further improve the existing water cooling system. Modifications to the lithography process used to do fine alignments of bi-crystals substrates and chrome masks, were also made and an additional modification has been done to improve the x-y stage of the AFM lithography stage by adding two 200 nm stepper motor stages.

Modifications were done to the cryogenic cooling systems; a susceptibility housing was constructed and a chip mounted shield was built for the low temperature facility. Finally, a new type of laser Josephson junction was made, tested and the work published [4].

The researcher was successful in designing and constructing changes that have upgraded the superconductor and nano-research group with minimal financial expenses. Research

in this field and improvements in techniques are ongoing.

List of References

- [1] M. Li and W. Anderson, "Laser annealing of laser assisted molecular beam deposited ZnO thin films with application to metal-semiconductor-metal photodetectors," *Journal of Applied Physics*, vol. 100, p. 053105, 2006.
- [2] [Online]. Available: <http://www.sintecoptronics.com/BeamAnalyser.htm>
- [3] W. van Staden, "The fabrication of pbco buffered step-edge josephson junctions," Master's thesis, University of Stellenbosch, 2006.
- [4] U. Buttner, G. Hardie, R. Rossouw, V. Srinivasu, and W. Perold, "Fabrication of submicron YBCO Josephson junctions by a sample mosaic navigation assisted laser etching process," *Superconductor Science and Technology*, vol. 20, pp. 426 – 429, 2007.
- [5] L. Doyle, G. Martin, T. Williamson, A. Al-Khateeb, I. Weaver, D. Riley, M. Lamb, T. Morrow, and C. Lewis, "Three-dimensional electron number densities in a titanium pld plasma using interferometry," *IEEE Transactions on Plasma Science*, vol. 27 No. 1, pp. 129 – 129, 1999.
- [6] T. Haugan, P. Barnes, L. Brunke, I. Maartense, and J. Murphy, "Effect of O2 partial pressure on YBa2Cu3O7-x thin film growth by pulsed laser deposition," *Physica C*, vol. 397, pp. 47 – 57, 2003.
- [7] J. Lopez, D. Blank, H. Rogalla, and J. Siejka, "Role of the oxygen plasma during in situ growth of YBaCuO thin films by pulsed laser deposition," *Physica C*, vol. 307, pp. 298 – 306, 1998.
- [8] H. de Villiers, "A process for the Manufacture of High Temperature Bi-epitaxial Josephson Junctions," Master's thesis, University of Stellenbosch, 2006.
- [9] P. Willmott, R. Timm, and J. Huber, "Reactive crossed beam scattering of a ti plasma and a n2 pulse in a novel laser ablation method," *Journal of Applied Physics*, vol. 82 (5), pp. 2082 – 2092, 1997.
- [10] K. Leung, "Radio frequency driven multicusp sources (invited)," *Review of Scientific Instruments*, vol. 69 No 2, pp. 998 – 1002, 1998.
- [11] D. Strachan, D. Smith, M. Fischbein, D. Johnston, B. Guiton, M. Drndic, D. Bonnell, and A. Johnson, "Clean electromigrated nanogaps imaged by transmission electron microscopy," *Nano Letters*, vol. 6, pp. 441 – 444, 2006.

- [12] A. Elkaseh, U. Buttner, M. Meincken, G. Hardie, V. Srinivasu, and W. Perold, "Nanoplough-Constrictions on Thin YBCO Films Made with Atomic Force Microscopy," *Journal of Nanoscience and Nanotechnology*, vol. 7, pp. 1 – 2, 2007.
- [13] L. Marty, A. Iaia, M. Faucher, V. Bouchiat, C. Naud, M. Chaumont, T. Fournier, and A. M. Bonno, "Self-assembled single wall carbon nanotube field effect transistors and AFM tips prepared by hot filament assisted CVD," *Thin Solid Films*, vol. 501, pp. 299 – 302, 2006.
- [14] J. Germain, M. Rolandi, S. Backer, and J. Frechet, "Sulfur as a Novel Nanopatterning Material: An Ultrathin Resist and a Chemically Addressable Template for Nanocrystal Self-Assembly," *Advanced Materials*, vol. 20, pp. 1 – 4, 2008.
- [15] R. von Pohl and P. Pringsheim, "Über die herstellung von metalspiegeln durch distillation im vakuum," *Verhandl. Deut. Physik*, vol. 14, p. 506, 1912.
- [16] V. L. Ginzburg and E. A. Andryushin, *Superconductivity*. World Scientific Publishing Co. Pte.Ltd., 1994.
- [17] F. F. Chen, *Introduction To Plasma Physics*, E. Epstein, Ed. Plenum Press, 1974.
- [18] T. Guo, P. Nikolaev, A. Thess, D. Colbert, and R. Smalley, "Catalytic growth of single-walled nanotubes by laser vaporization," *Chemical Physics Letters*, vol. 243, pp. 49 – 54, 1995.
- [19] E. Rexer, M. Joshi, R. DeLeon, P. Prasad, and J. Garvey, "A reactive laser ablation source for the production of thin films," *Review of Scientific Instruments*, vol. 69, pp. 3028 – 3030, 1998.
- [20] R. DeLeon, M. Joshi, E. Rexer, P. Prasad, and J. Garvey, "Progress in thin film formation by laser assisted molecular beam deposition. (LAMBD)," *Applied Surface Science*, vol. 127, pp. 321 – 329, 1998.
- [21] R. Kang, K. Wang, J. Wang, and D. Guo, "Removal of scratch on the surface of MgO single crystal substrate in chemical mechanical polishing process," *Applied Surface Science*, vol. 254, pp. 4856 – 4863, 2008.
- [22] A. Abert, J. Contour, A. Defossez, D. Ravelosona, W. Schwegle, and P. Ziemann, "Critical thickness of ybaco (123) strained thin films and superlattices grown by pulsed laser deposition," *Applied Surface Science*, vol. 96 - 98, pp. 703 – 707, 1996.
- [23] F. Graser, "A reproducible design and manufacturing process for squid magnetometers," Master's thesis, University of Stellenbosch, 2005.
- [24] A. A. Elkaseh, "Fabrication of high-temperature superconducting nanobridges using atomic force microscopy," Master's thesis, University of Stellenbosch, 2006.
- [25] H. Schneidewind, F. Schmidl, S. Linzen, and P. Seidel, "The possibilities and limitations of ion-beam etching of yba2cu3o7 thin films and microbridges," *Physica C*, vol. 250, pp. 191 – 201, 1995.

- [26] P. Rottier, "Establishing a Process for the Fabrication of High Quality HTc SQUIDS," Master's thesis, University of Stellenbosch, 2002.
- [27] G. Koren, A. Gupta, R. Baseman, M. Lutwyche, and R. Laibowitz, "Laser wavelength dependant properties of $\text{YBa}_2\text{Cu}_3\text{O}_{7-d}$ thin films deposited by laser ablation," *Applied Physics Letters*, vol. 55, pp. 2450 – 2452, 1989.
- [28] S. Kuriki, K. Takahashi, Y. Kawaguchi, M. Matsuda, and T. Otowa, "High critical current density YBCO films and fabrication of DC-SQUIDS," *Superconductor Science and Technology*, vol. 15, pp. 1693 – 1697, 2002.
- [29] D. Zhu, J. Huang, H. Li, M. Shen, and X. Su, "A new method to preserve the c-axis growth of thick $\text{YBa}_2\text{Cu}_3\text{O}_{7-d}$ films grown by pulsed laser deposition," *Physica C*, vol. 469, pp. 1977 – 1982, 2009.
- [30] B. Dam, J. Rector, M. Chang, S. Kars, D. deGroot, and Griessen, "Laser ablation threshold of $\text{YBa}_2\text{Cu}_3\text{O}_{6+x}$," *Applied Physics Letters*, vol. 65 (12), pp. 1581 – 1583, 1994.
- [31] E. Conradie, "The Design and Fabrication of DC-SQUID Magnetometers," Master's thesis, University of Stellenbosch, 1998.
- [32] J. Thompson, B. Hyde, R. Withers, J. Anderson, J. F. Gerald, J. Bitmead, and M. Paterson, " $\text{YBa}_2\text{Cu}_3\text{O}_{7-x}$ atmospheric degradation of the high-temperature superconductor." *Materials Research Bulletin*, vol. 22, pp. 1715 – 1724, 1987.
- [33] F. Herbstritt, T. Kemen, A. Marx, and R. Gross, "Ultraviolet light assisted oxygenation process for submicron $\text{YBa}_2\text{Cu}_3\text{O}_{7-d}$ thin film devices," *Journal of Applied Physics*, vol. 91, pp. 5411 – 5418, 2002.
- [34] M. A. A. Aliabadi, Y. A. Farshchi, "A new Y-based HTSC with T_c above 100 K," *Physica C*, vol. 469, pp. 2012 – 2014, 2009.
- [35] A. Fasasi, R. Bucher, B. Ngom, U. Buttner, M. Maaza, C. Theron, and E. Rohwer, "Structural and optical properties of annealed W-doped BaTiO_3 thin films prepared by pulsed laser deposition," *Journal of Physics and Condensed Matter*, vol. 19, pp. 466 214 – 466 225, 2007.
- [36] A. Fasasi, M. Maaza, E. Rohwer, D. Knoessen, C. Theron, A. Leitch, and U. Buttner, "Effect of Zn-doping on the structural and optical properties of BaTiO_3 thin films grown by pulsed laser deposition," *Thin Solid Films*, vol. 516, pp. 6226 – 6232, 2008.
- [37] A. Fasasi, M. Maaza, C. Theron, P. Neethling, U. Buttner, A. Leitch, and A. Chaudhary, "Non-linear absorption and second harmonic imaging of Zn- BaTiO_3 thin films prepared by laser ablation," *Thin Solid Films*, vol. 516, pp. 6233 – 6239, 2008.
- [38] A. Gupta and B. Hussey, "Laser deposition of $\text{YBa}_2\text{Cu}_3\text{O}_{7-d}$ films using a pulsed oxygen source," *Applied Physics Letters*, vol. 58, pp. 1211 – 1213, 1991.

- [39] P. Willmott, H. Spillmann, and J. Huber, "Design and synthesis of novel thin films and structures by reactive crossed-beam laser ablation," *Journal of Materials Chemistry*, vol. 12, pp. 397 – 402, 2002.
- [40] A. Westerheim, L. Yu-Jahnes, and A. Anderson, "Off-axis magnetron sputtering of ybco films: the influence of atomic oxygen," *IEEE Transactions on Magnetics*, vol. 27, pp. 1001 – 1005, 1991.
- [41] T. M. Z. Petrovic, *Plasma Electronics: applications in Microscopyelectronic Device Fabrication*, S. Cowley, Ed. CRC Press Taylor & Francis Group, 2006.
- [42] Q. Ji and T. King, "Production of various species of focused ion beam," *Review of Scientific Instruments*, vol. 73 No 2, pp. 822 – 824, 2002.
- [43] F. Tian, G. Yang, J. Bai, J. Xu, C. Hou, Y. Liang, and K. Wang, "Laser direct writing using submicron-diameter fibers," *Optical Society of America*, vol. 17 No 22, pp. 19 960 – 19 968, 2009.
- [44] B. Ngoma, T. Mpahane, N. Manyala, O. Nemraoui, U. Buttner, J. Kana, A. Fasasi, M. Maaza, and A. Beye, "Structural and optical properties of nanostructured tungsten-doped ZnO thin films grown by pulsed laser deposition," *Applied Surface Science*, vol. 255, pp. 4153 – 4158, 2009.
- [45] E. Coetsee, H. Swart, J. Terblans, O. Ntwaeaborwa, K. Hillie, W. Jordaan, and U. Buttner, "Characterization of Y2SiO5:Ce thin films," *Optical Materials*, vol. 29, pp. 1338 – 1343, 2007.
- [46] A. Fasasi, B. Ngom, J. Kana-Kana, R. Bucher, M. Maaza, C. Teron, and U. Buttner, "Synthesis and characterisation of Gd-doped BaTiO3 thin films prepared by laser ablation for optoelectronic applications," *Journal of Physics and Chemistry of Solids*, vol. 70, pp. 1322 – 1329, 2009.
- [47] G. Hardie, U. Buttner, and W. Perold, "The Enhancement of Superconducting YBa2Cu3O7-x Thin Films by Electric Field Application During Deposition," *IEEE Transactions on Applied Superconductivity*, vol. 19, pp. 3387 – 3390, 2009.
- [48] W. van Staden, U. Buttner, V. Srinivasu, and W. Perold, "A novel buffered high-Tc superconducting step-edge Josephson junction," *Superconductor Science and Technology*, vol. 20, pp. 419 – 425, 2007.

Appendices

Plasma Laser Deposition Procedure

Before starting any deposition the logbook must be filled out, and then the Laser may be switched on. After 15 min the water is switched on, and the high voltage of the laser can be switched on and set to to the desired voltage (24Kv). Now the sample must be mounted into the chamber.

Chamber Preparation and Sample Mounting

1. The chamber is kept under vacuum when not in use.
2. Nitrogen gas is used when venting the vacuum chamber.
3. Gloves should be worn while mounting the substrate and doing any work in the chamber.
4. The main flange with the substrate holder is removed and the substrate is mounted using silver paste. Care is taken not to contaminate the surface of the substrate.
5. After mounting the substrate, the flange is placed back onto the chamber and the bolts are attached.
6. Before closing the top vacuum chamber lid, the laser position and spot size must be characterized. Eye-wear must be worn during this procedure. Also, the laser energy must be measured with a pyroelectric sensor. This measurement is done where the laser beam exits the laser unit.

Pump Down Procedure

1. Once the laser has been quantified, the substrate heater is temporarily switched on and checked. This is just to confirm that the temperature sensor and heater element are still intact.
2. The top chamber lid can be closed, the bypass valve opened and the roughing pump and pressure gauge are switched on.

3. The bypass valve is closed when a pressure of 1 mbar has been reached.
4. The main vacuum valve to the turbo molecular pump (TMP) can be opened and the water cooling to the TMP can be switched on. Note: Do not switch the TMP on before an initial pressure of 1 mbar has been reached and the main TMP valve has been opened.
5. Keep track of the pressure until it is clear that the vacuum is improving.
6. After 2 hrs the pressure should have reached 4×10^{-5} mbar.
7. The substrate heater can now be switched on.
8. Check that the temperature of the TMP. This is just an extra precaution to check that the water cooling is on.

Deposition Process

1. Set reactive gas (if used) to correct deposition pressure and check the substrate temperature.
2. Make sure the shutter is covering the substrate and switch on the target rotation.
3. Now pre-ablate for 3 minutes, checking that laser position, plume, pressure, pulse rate and substrate temperature are correct.
4. Now the shutter can be opened and the deposition can start.
5. Keep checking all parameters regularly.

Ending a Deposition Process

1. Once the deposition time has been met, the laser beam is switched off.
2. The reactive gas valve inlet can now be closed.
3. Thereafter the main TMB valve can be closed and the TMP can be switched off.
4. The TMP water cooling is switched off.
5. Note! The bypass valve to the chamber must be closed. It is important to do this before the main chamber is vented. Failing to close the bypass valve and then venting the chamber could result in damage to the TMP.

6. Depending on the material that was deposited, an annealing process might be needed (YBCO). The gas (oxygen) pressure is then set by opening the gas inlet valve again and pressurizing the chamber to the necessary pressure.
7. Once the annealing is complete, the substrate heater can be switched off.
8. The main chamber can be vented once the substrate has cooled down to room temperature.

Shutdown Procedure

1. The substrate holder flange is taken off the chamber, and the substrate is removed.
2. Thereafter the substrate holder flange is refitted, and the chamber is placed under vacuum. This is done by re-opening the chamber bypass valve and switching on the roughing pump.
3. Once the deposition chamber is under vacuum, the bypass valve is closed again, and the roughing pump is switched off.
4. Now all the instrumentation used can be switched off.
5. The laser startup and shutdown instructions are given on the main control unit.

ICM Operating Procedures

Chamber Preparation and Sample Mounting

The same vacuum system is used for the ICM and the Argon ion mill, so the start-up procedures are identical.

1. Close the valves to both the roughing and diffusion pumps and vent the ICM system.
2. Remove power supply cable connections from the ICM-head.
3. Do a physical check of the target, if necessary use fine sand paper to clean cylindrical target.
4. Check thermocouple is in place and the temperature controller is set to correct temperature profile.
5. Clean substrate heater surface before mounting clean MgO substrate.
6. Check that the heater assembly is firmly mounted on the water-cooled base. Centre the heater, using the chamber walls as a reference.
7. Make sure the heater temperature is below 30°C. Apply a thin layer of silver paste and place the substrate firmly onto the substrate heater.
8. Position the sample on the substrate heater and apply pressure to the edges of the substrate for even coverage of the silver paste.
9. Clean O-rings between chamber and ICM head. Apply a thin layer of vacuum grease.
10. Position the ICM-head onto the deposition chamber.

Starting a Deposition Process

1. Close the gas valves between the argon and oxygen gas cylinders and open the gas valves on the workbench. This opens up the gas feeds to the vacuum chamber, allowing one to test if there are any leaks in the gas lines.
2. Change the roughing valve to backing position, switch on the diffusion pump and its water cooling, and wait 15 minutes.
3. Turn the valve to roughing and switch on vacuum pump. When the pressure has reached 20 Torr, then open the diffusion pump valve.
4. Switch high vacuum gauge on. Wait (15 minutes) until vacuum reaches 8.10^{-6} mbar.
5. Close the workbench gas inlet valves and open the primary and secondary valves on both gas cylinders.
6. The diffusion pump is closed during deposition (diffusion pump may be switched off if only one deposition is done), return the valve position to roughing. The chamber pressure should stabilize at 1×10^{-2} mbar.
7. Set both gas mixtures by adjusting the workbench gas inlet valves (typically 2:1 oxygen to argon) reaching a total pressure of between 150-225 mm Hg.
8. Switch water cooling to ICM, by using the in line valves, and switch on the water cooling. This cools the magnets and heater; also check that there are no water leaks.
9. Switch on the temperature controller and wait until a temperature of 740°C has been reached.

ICM Operation

1. Connect the negative terminal to the copper water cooling pipes, which are the ICM cathode. The positive terminal to the ICM anode, which is the aluminium housing, can also be grounded.
2. Switch on the constant current power supply, and set the voltage to 350 V DC and 40 mA until plasma ignition, thereafter lower the voltage to 200 V DC and slowly increase the current to 400 mA.
3. Sputtering has started and the deposition rate is between 2 nm to 4 nm, depending on the final pressure setting. The deposition thickness is a function of the deposition time.

Ending a Deposition Process

1. After the deposition, switch off sputtering power supply.
2. Close only the argon workbench gas inlet valve.
3. The temperature profile is set to anneal at 500°C at 3°C per minute.
4. Slowly increase the oxygen flow to the chamber by adjusting the oxygen workbench inlet valve. At 550°C, change the rouging pump valve to backing or forline pump setting. This disables the pump and the oxygen can reach atmospheric pressure.
5. Keep at 500°C during the annealing process. The chamber pressure should now be about 1 bar.
6. The temperature is kept at 500°C for 1 h, thereafter the heater is turned off.
7. Once the heater temperature has reached 300°C, the oxygen workbench gas feed valves, as well as at the gas cylinder, can be closed.
8. Remove DC power supply cable connections from the ICM, and lift off the ICM-head, after substrate heater is at room temperature.

System Shutdown

1. Replace ICM head on the top vacuum chamber.
2. Turn the main valve to the roughing position. The ICM should always be kept under vacuum if not in use.
3. Close the main valve by positioning either to the forline, or centre position, once sufficient vacuum (100-50 Torr) has been reached.
4. Switch the diffusion pump off, also the roughing pump and the workbench gauges.
5. Return the roughing pump exhaust pipe into the room, and close the window.
6. Wait 20 minutes before turning off the water cooling to the diffusion pump.

Ion Argon Mill Procedure

Start Up Procedure

1. Turn the water cooling to the diffusion pump on.
2. Verify that the roughing pump exhaust pipe is positioned so that the fumes can exit the room.
3. Turn on the diffusion pump and the roughing pump (valve of the diffusion pump is closed and the main valve is turned to the backing position).
4. Wait for 15 minutes for the diffusion pump to heat up.

Mounting Sample Into Mill

1. The argon ion mill is kept under vacuum. Position the main valve to the foreline pumping position and vent the system through the vent valve switch of the workbench.
2. Remove the RF and high voltage; positive, negative and earth connections.
3. Move the head of the argon ion mill carefully to avoid excessive bending of the water pipes, onto the elevated platform next to the mill.
4. Place the substrate onto the sample-holder using tweezers, and coupling the substrate using heat-sink paste . Keep the substrate surface clean and do not use too much paste.
5. Orientate the sample holder tilt angle and rotational angle according to milling requirements.
6. Check the bottom chamber o-ring to make sure that no particles gathered there during the process of sample mounting. Remove such particles and reapply vacuum grease if necessary.
7. Reposition the argon ion mill head on top of the vacuum chamber.

8. Position the RF shield over the argon ion mill, reconnect the RF and high voltage cables.

Starting an Etch Process

1. The positive HV is connected to the top grid connector mounted on the plasma chamber head. For low etch rate mode, the negative HV cable is connected to the middle grid and ground cable to the bottom grid. For high etch rates, reverse the negative HV and ground connections.
2. Close the side valve on the argon gas cylinder and open the workbench gas inlet valve. This will ensure that the gas feed has no contaminant gases in the pipe after pump down.
3. Turn the main valve to roughing. Wait for the pressure to reach 20 Torr.
4. Change the main valve to the backing position. This now backs the diffusion pump. Now open the diffusion pump valve.
5. Switch the high vacuum gauge on. Wait for the vacuum to reach 2×10^{-5} mbar. This should take about 15 minutes.
6. Switch on the water cooling to the magnets and sample holder while checking that there are no water leaks.
7. Close the argon gas inlet valve on the workbench. Open the primary and secondary valves at the argon gas cylinder.
8. Optional: Flush the system with argon gas regulated by the gas inlet on the workbench.
9. Place the cover of the mill over it to serve as protection against RF radiation.
10. Adjust the gas workbench inlet valve to obtain a chamber pressure of 2×10^{-4} mbar.
11. Switch on the RF source input power to 50 W. Obtain impedance matching by adjusting the two variable capacitors until a plasma is seen (through viewing window). The reflected power should preferably be below 5 W.
12. The high voltage is now activated and set to the desired values (+1000 V and -1000 V).
13. The substrate is now milled for the desired time period (at 2 nm - 3 nm per minute).
14. When milling Josephson junctions, extra care must be taken not to lose superconductivity during this step.

Sample Removal

1. Turn off the high voltage supply.
2. Turn off the RF source.
3. Close the gas valves on the workbench and at gas (argon) cylinder.
4. Switch off the closed water cooling system of the mill head.
5. Take off the RF shield of the mill, remove the high voltage cables and earth cable.
6. Close the diffusion pump to chamber valve and turn the main valve to the backing position.
7. Switch off the high vacuum gauge and then vent the system.
8. Remove the mill head and position back on elevated block.
9. Inspect sample and remove if etching is complete.

System Shutdown

1. Replace the top of the ion argon mill back onto the vacuum chamber.
2. Turn the main valve to the roughing position. The mill is kept under vacuum if not in use.
3. Change main valve to backing position, if sufficient vacuum (100-50 Torr) has been reached.
4. Switch off both the diffusion and the roughing pumps and the workbench gauges.
5. Return the roughing pump exhaust pipe inside the room and close the window.
6. Wait 20 minutes before turning off the water cooling of the diffusion pump.

Photolithography

Process Optimization

1. If possible check the UV light intensity before starting. For repeatability purposes the energy is calculated.
2. The base of the exposure unit was coated with a photo-absorbent material. This significantly improved the resist resolution obtained with MgO substrates, limiting light reflections and the occurrence of standing waves.
3. Shadowing of the resist profiles occurred frequently. This problem was addressed by removing excess resist (edge beads) from the corner regions to make a gap free contact possible.
4. The gap between mask and resist was, accordingly minimised to ensure sufficient contact pressure to avoid diffraction.
5. New resist and developer were purchased and process times optimised.

The resist used in this research was SPR 700 and a MF 24A developer. This resist was used for its better dry etching properties and ability to withstand higher temperatures without compromising resolution.

Optimal Parameters For The SPR 700 Photoresist and MF24A Developer

1. Resist Spinning 4500 rpm for 50 s
2. Soft Bake 90 s at 115°C
3. Soft Bake cool down 5 min
4. UV Exposure MgO: 21 s, YBCO/PBCO: 25 s

5. Post Exposure Wait 10 min
6. Development MgO: 54 s, YBCO/PBCO: 25 s
7. DI Immersion 30 s rinse
8. Hard Bake 5 min at 95°C

Laser Junction results

Laser Junctions

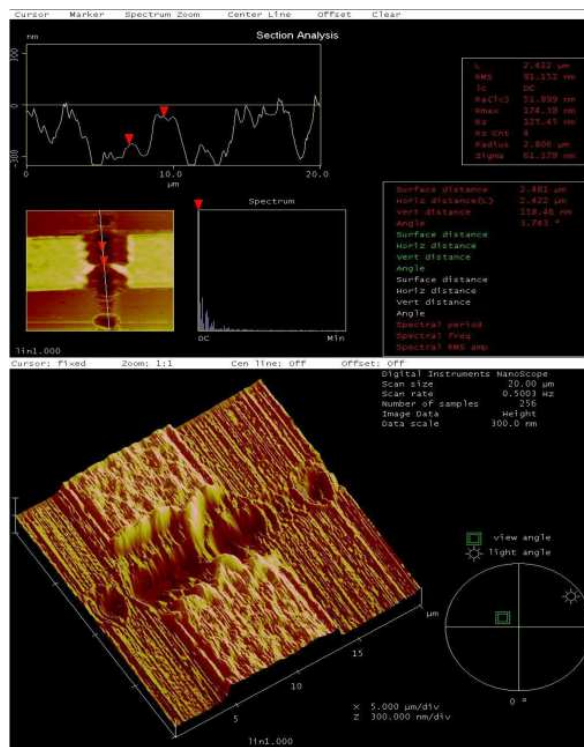


Figure 1: First attempts at laser junction. Legs 1 and 2 were not successful

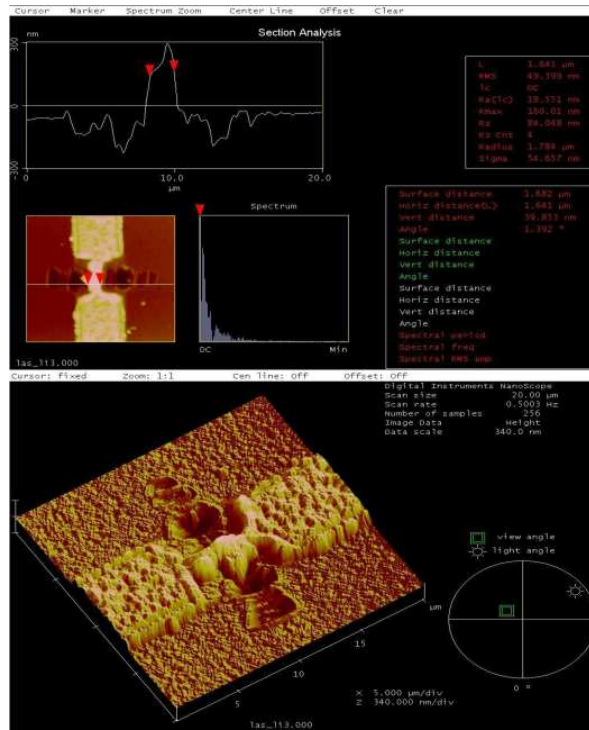


Figure 2: Laser junction leg 3 width measured 1.641 μm



Figure 3: Laser junction leg 3 (1.641 μm) Shapiro steps at 57.1K and 9.073 GHz

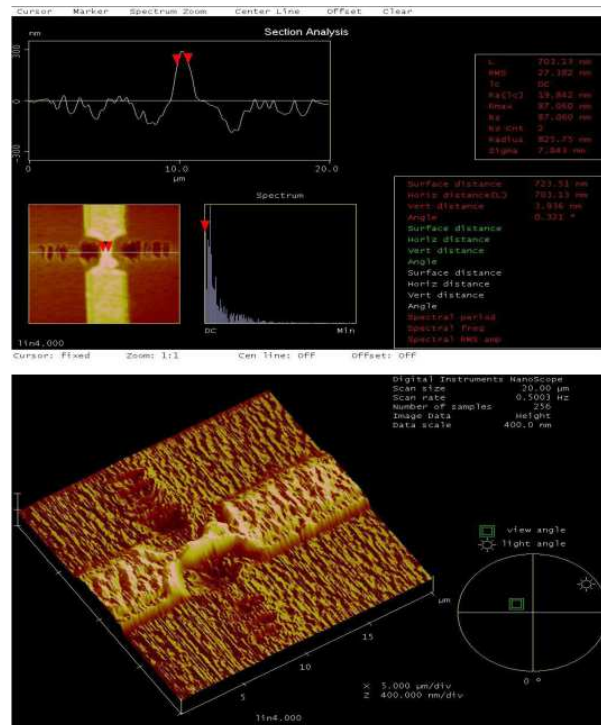


Figure 4: Laser junction leg 4 width measured 703.13 nm

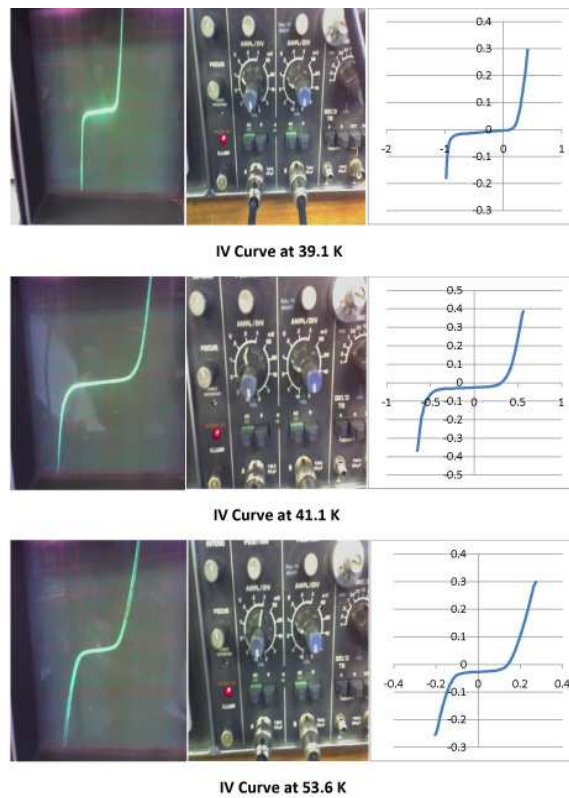


Figure 5: Laser junction leg 4 IV curve at different temperatures

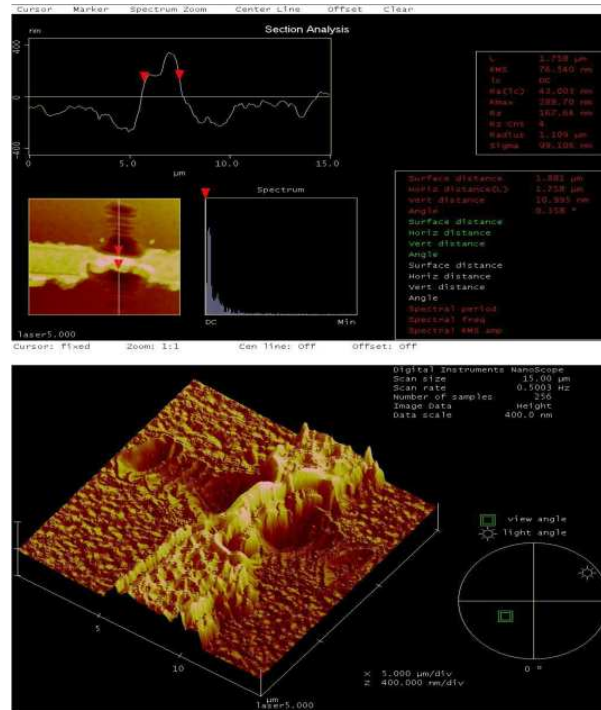


Figure 6: Laser junction leg 5 width measured 1.758 μm

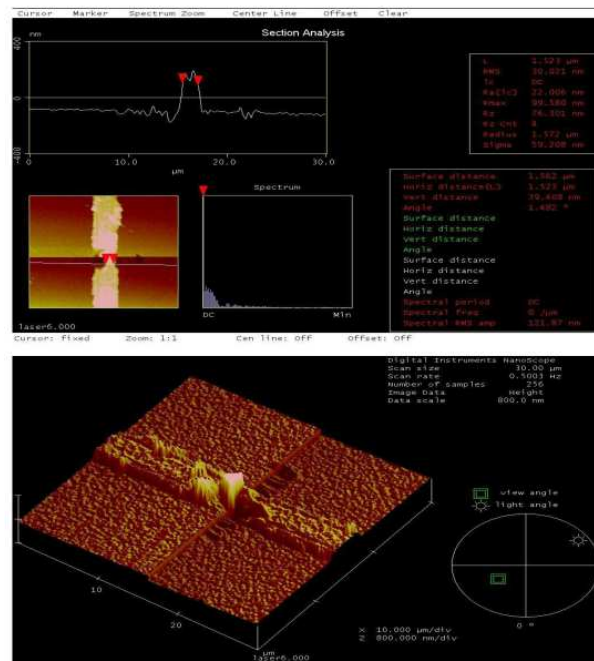


Figure 7: Laser junction leg 6 width measured 1.523 μm

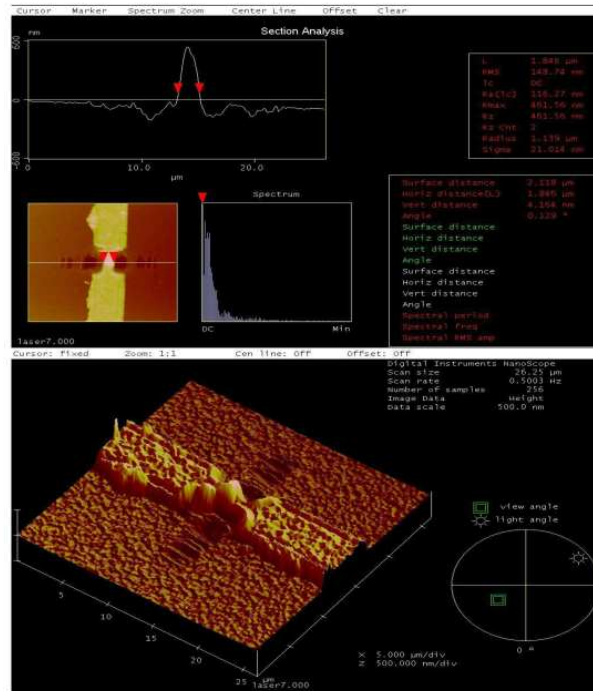


Figure 8: Laser junction leg 7 width measured 1.846 μm

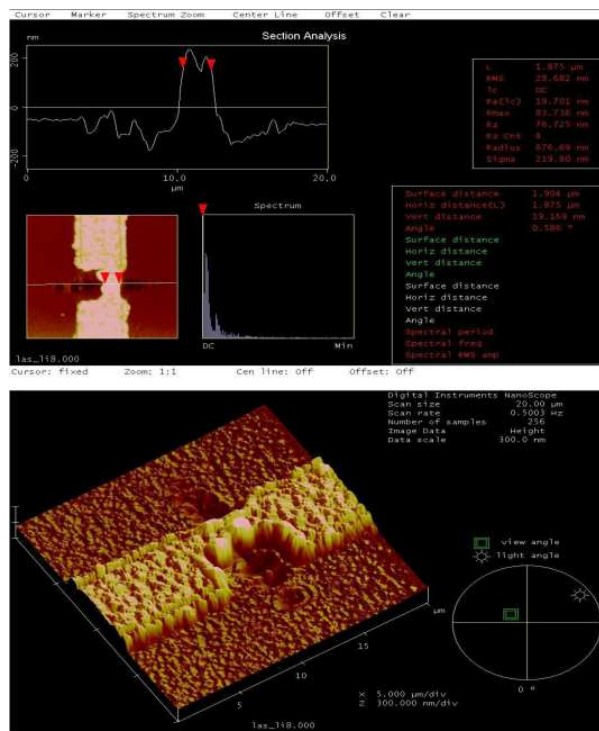


Figure 9: Laser junction leg 8 width measured 1.875 μm

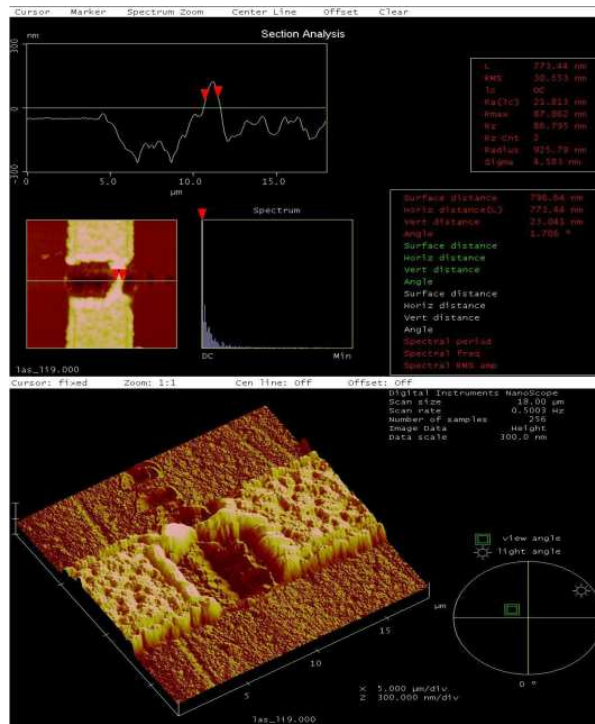


Figure 10: Laser junction leg 9 width measured 773,44 nm

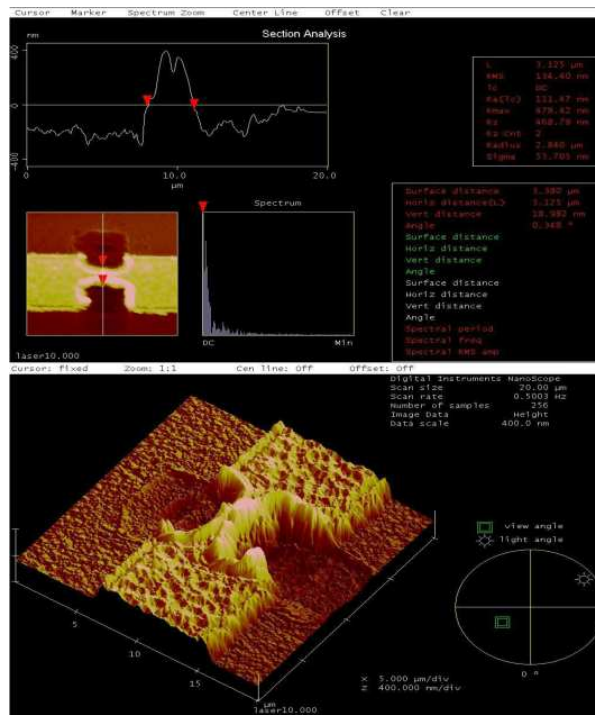
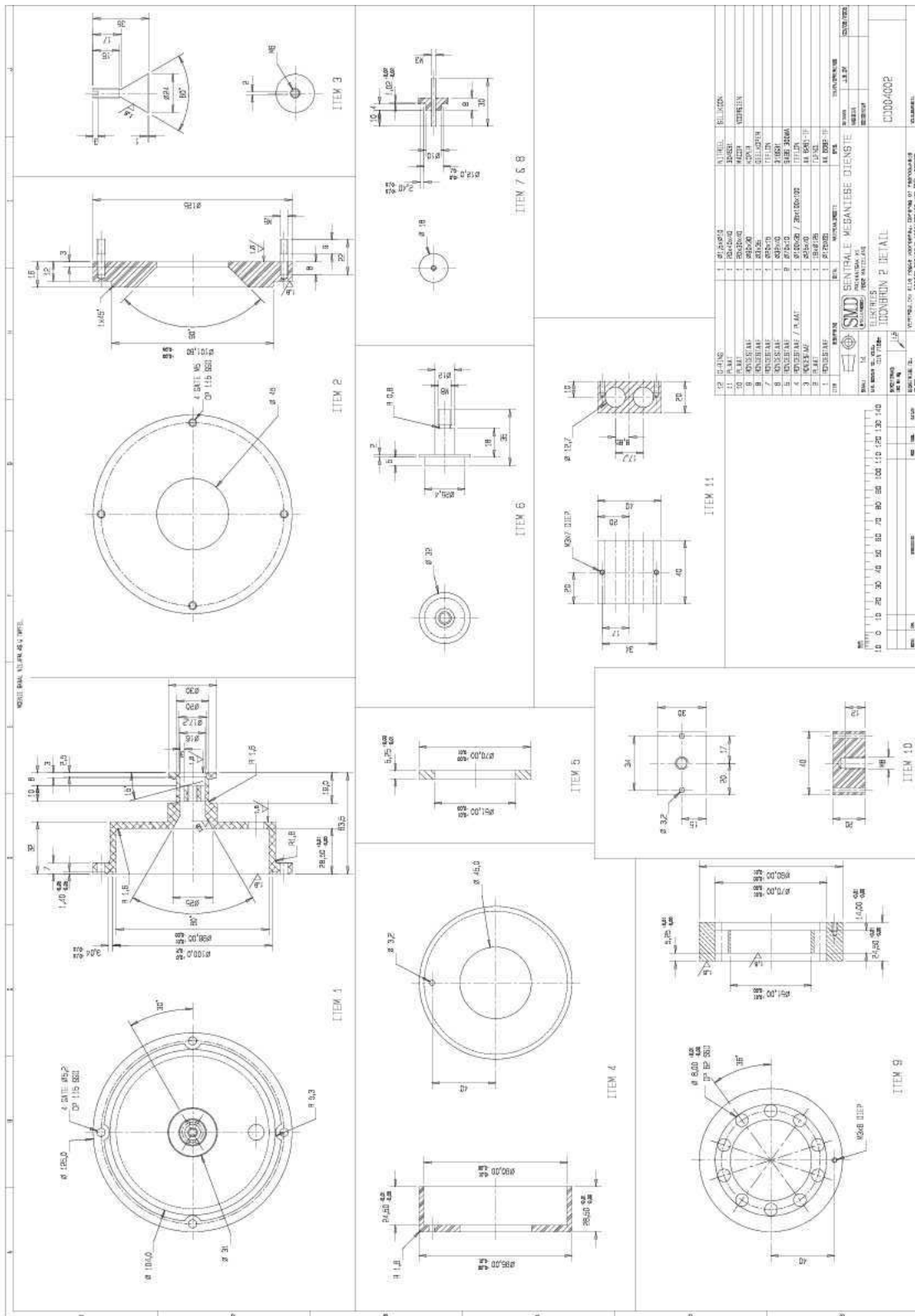


Figure 11: Laser junction leg 10 width measured 3.125 micrometers

Technical Diagrams



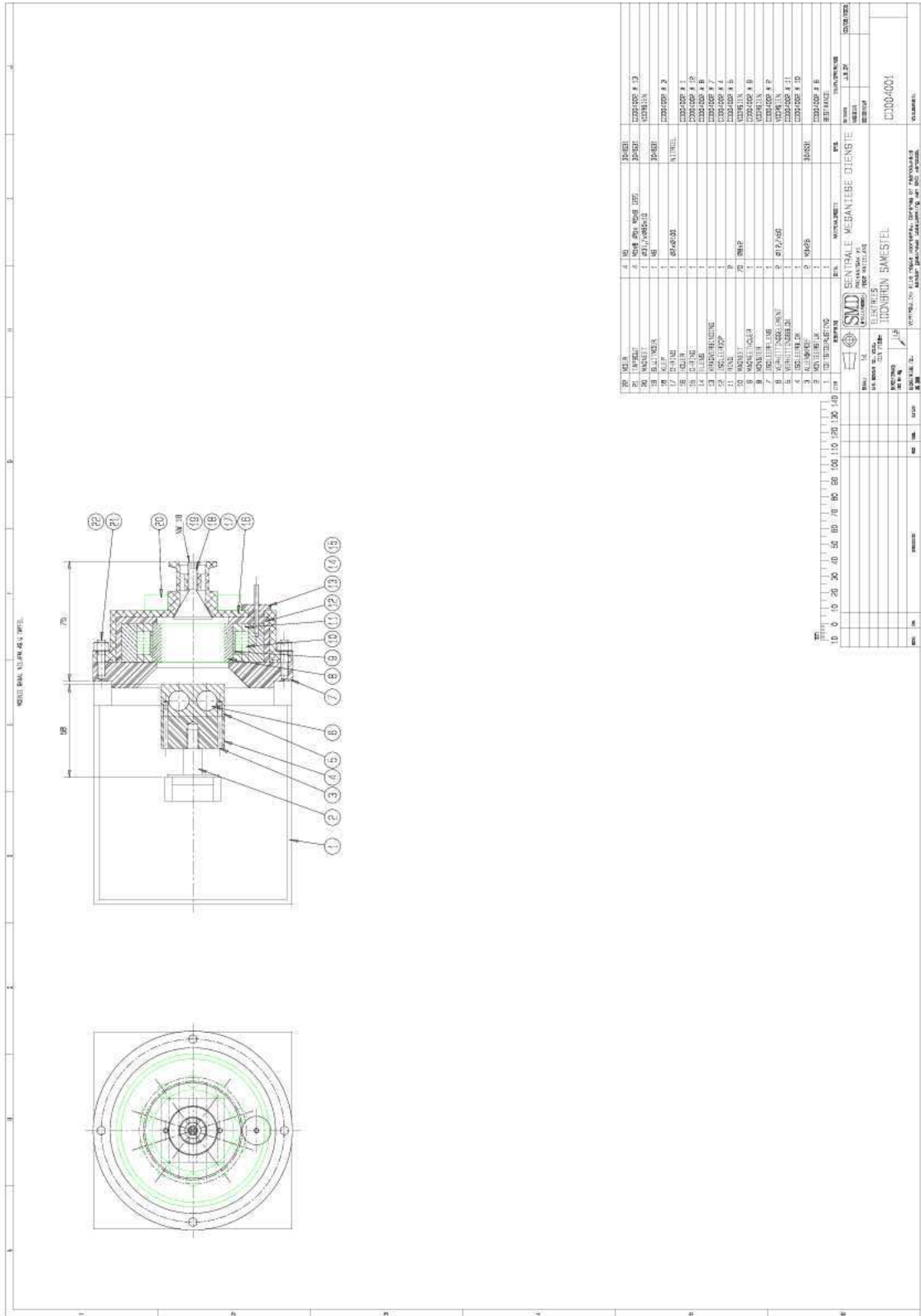


Figure 15: ICM complete

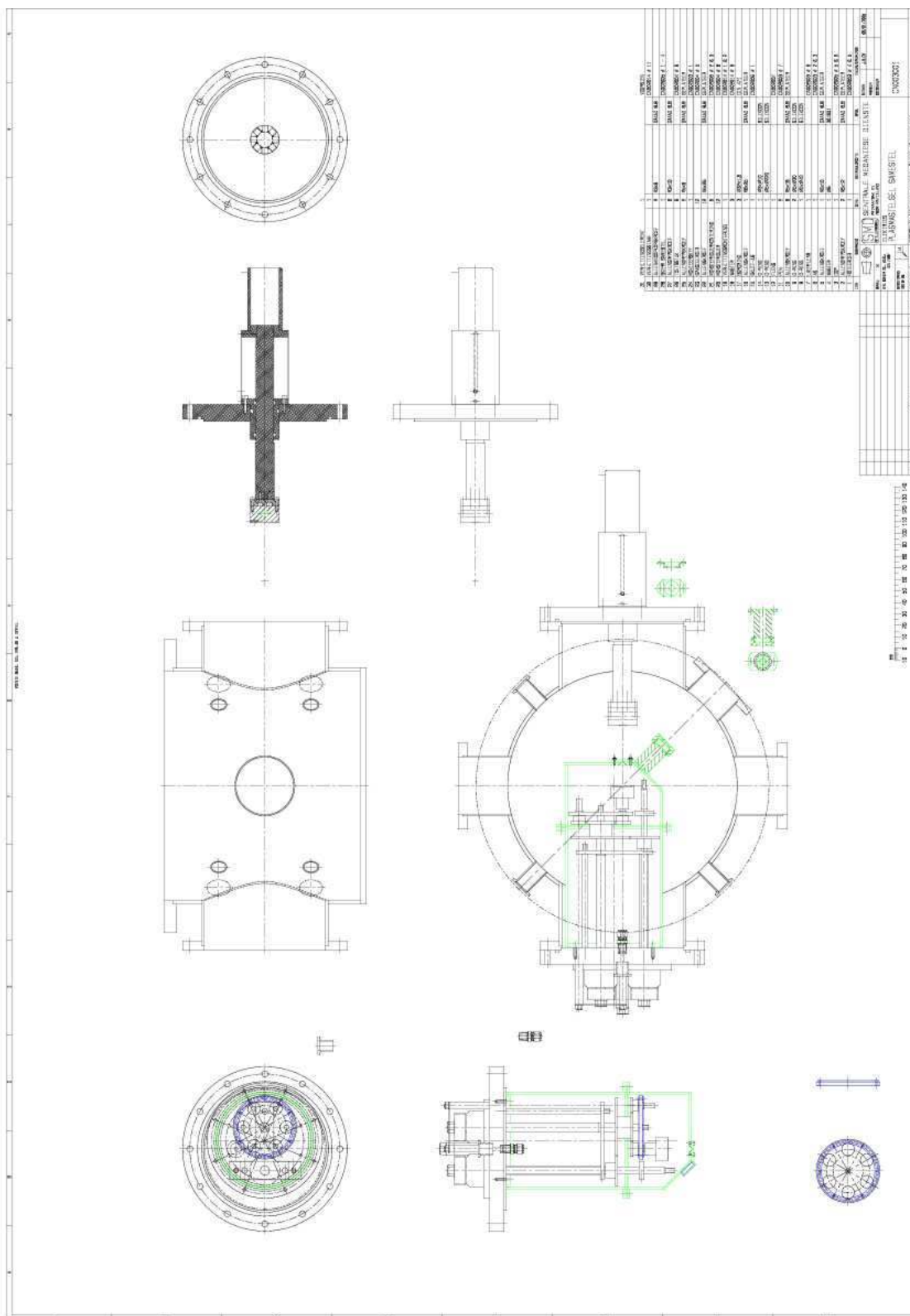


Figure 16: Laser assisted molecular beam deposition detail

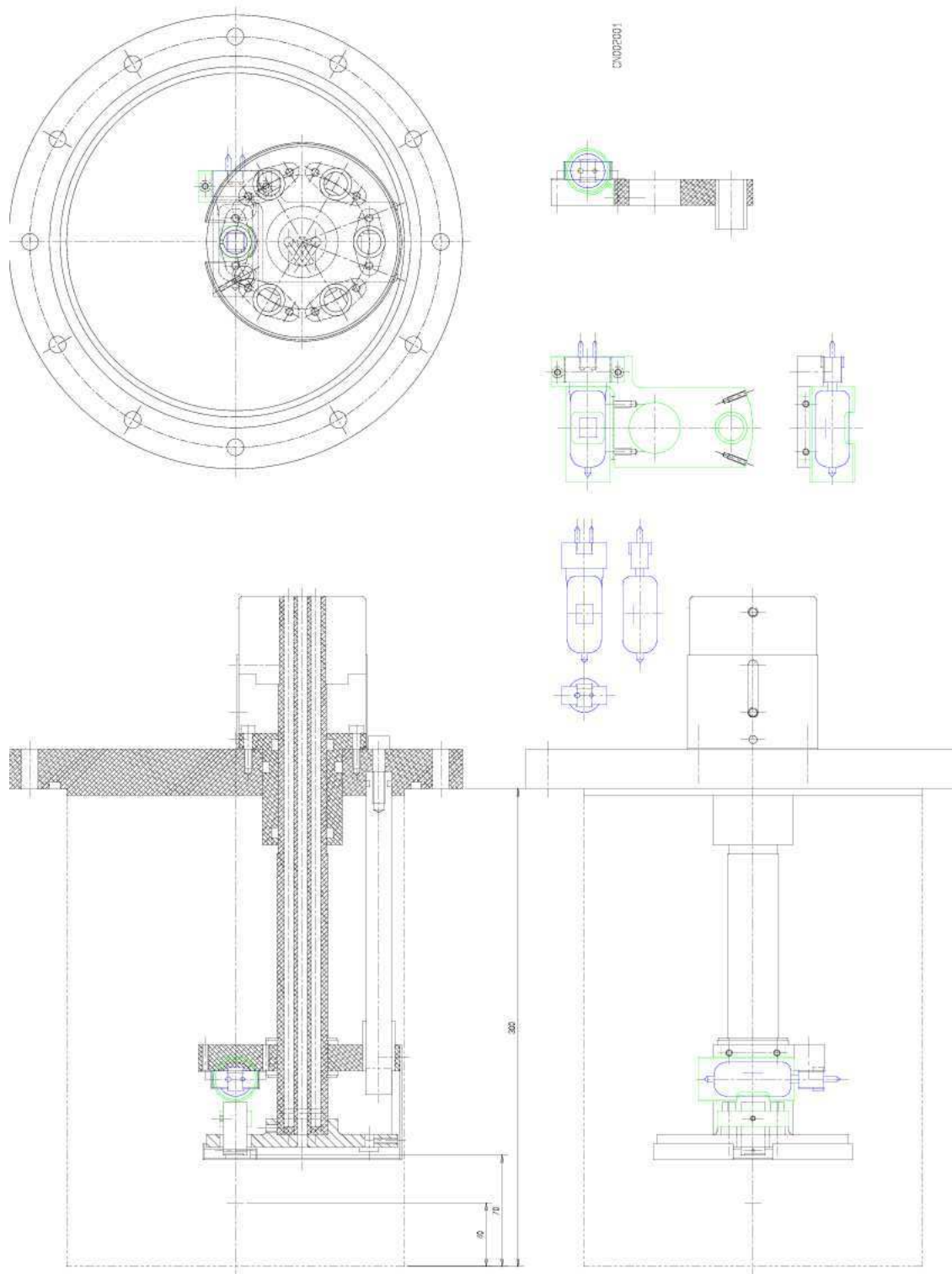


Figure 24: Six substrate holder assembly detail

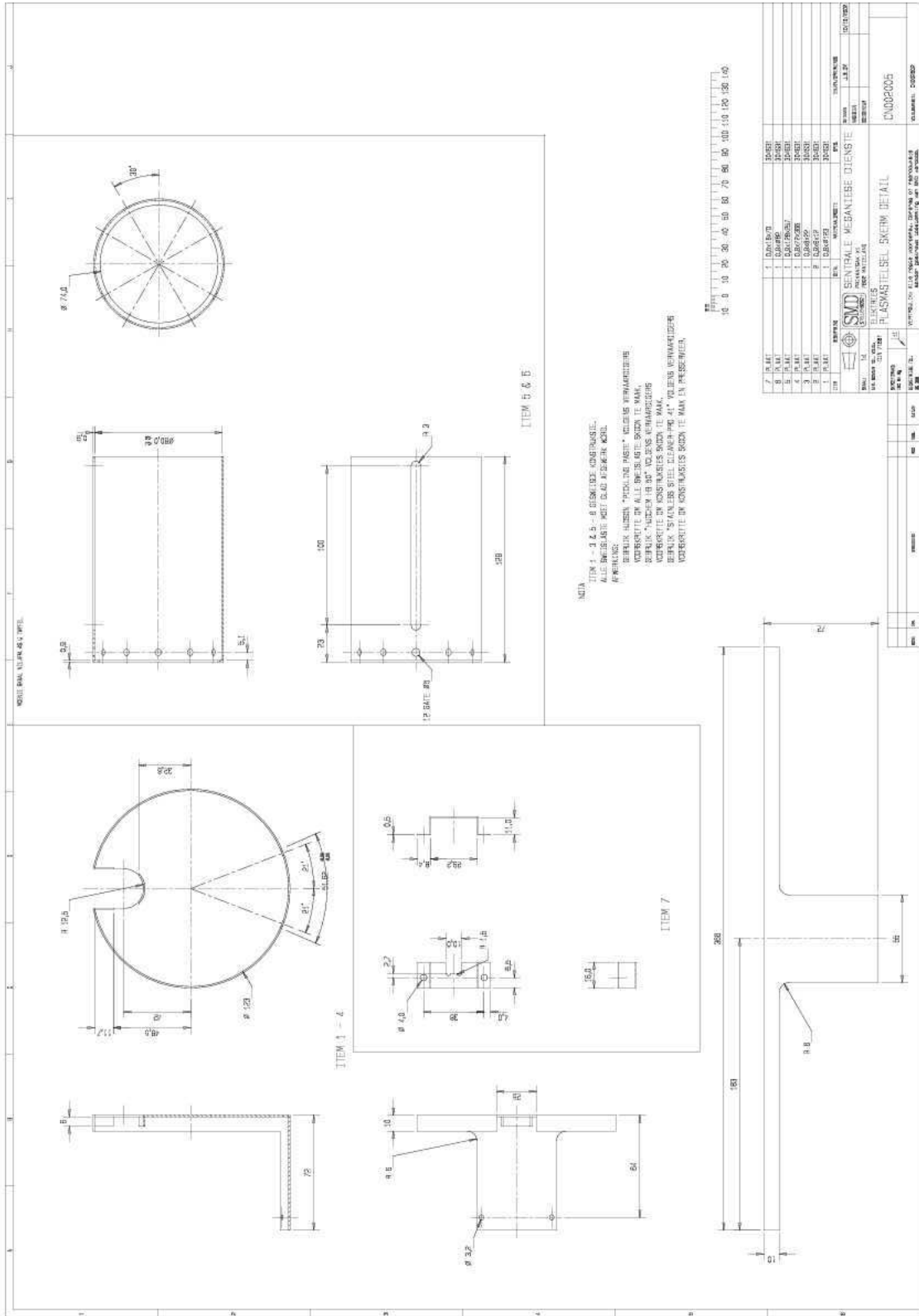


Figure 27: Six substrate holder shield assembly design

